A genetic screen identifies *dreammist* as a regulator of sleep

Ida L. Barlow[1,2], Eirinn Mackay[1,3], Emily Wheater[1,4], Aimee Goel[1], Sumi Lim[1], Steve Zimmerman[5], Ian Woods[6], David A. Prober[7], and Jason Rihel[1,*]

[1] Department of Cell and Developmental Biology, University College London, UK;

[2] Current address: MRC London Institute for Medical Sciences, Imperial College London, UK

[3] Current address: Sainsbury Wellcome Centre for Neural Circuits and Behaviour, University College London, UK

[4] Current address: MRC centre for Reproductive Health, University of Edinburgh, UK

[5] Department of Molecular and Cellular Biology, Harvard University, USA

[6] Ithaca College, New York, USA

[7] Division of Biology and Biological Engineering, California Institute of Technology, Pasadena, USA

* Lead author: Jason Rihel j.rihel@ucl.ac.uk

Significance statement: Sleep is an essential component of behaviour, but the genes that regulate sleep and wake states are still being uncovered. A viral insertion screen in zebrafish identified a novel sleep mutant called *dreammist*, in which a small, highly-conserved transmembrane protein is disrupted. The discovery of *dreammist* highlights the importance of a class of small transmembrane-protein modulators of the sodium pump in setting appropriate sleep duration.

ABSTRACT

Sleep is a nearly universal feature of animal behaviour, yet many of the molecular, genetic, and neuronal substrates that orchestrate sleep/wake transitions lie undiscovered. Employing a viral insertion sleep screen in larval zebrafish, we identified a novel mutant, *dreammist* (*dmist*), with altered sleep-wake dynamics. CRISPR/Cas9-mediated disruption of *dmist* also led to behavioural hyperactivity and reduced sleep at night. The neuronally expressed *dmist* gene is conserved across vertebrates and encodes a small single-pass transmembrane protein that is structurally similar to the Na^+,K^+-ATPase regulator, FXYD1/Phospholemman. Disruption of either *fxyd1* or *atp1a3a*, a Na^+,K^+-ATPase alpha-3 subunit associated with several heritable movement disorders in humans, led to decreased night-time sleep. As intracellular Na^+ concentration is disrupted in *dmist* mutant brains after high neuronal activity similarly to *atp1a3a* mutants, but is also elevated specifically at night, we propose that sleep-wake stability is modulated by Dmist-dependent changes to Na^+ pump function during sleep homeostatic challenge and at specific times of the day-night cycle.

INTRODUCTION

The ability for animals to switch between behaviourally alert and quiescent states is conserved across the animal kingdom (Cirelli, 2009; Joiner, 2016). Fundamental rules that govern the regulation of sleep-like states are shared across species, such as the role of circadian and homeostatic cues in regulating the time and amount of sleep, stereotyped postures, heightened arousal thresholds, and the ready reversibility to a more alert state (Joiner, 2016). The near ubiquity of behavioural sleep implies that it serves ancient functions and is subject to conserved regulatory processes. However, many key molecular components that modulate sleep and wake states remain undiscovered.

Over the past two decades, investigations into sleep and arousal states of genetically tractable model organisms, such as *Drosophila melanogaster*, *C. elegans*, and zebrafish have

uncovered novel molecular and neuronal components of sleep regulation through gain- and loss-of-function genetic screens (reviewed in Barlow and Rihel, 2017; Sehgal and Mignot, 2011). The power of screening approaches is perhaps best exemplified by the first forward genetic sleep screen, which identified the potassium channel *shaker* as a critical sleep regulator in Drosophila (Cirelli et al., 2005). This result continues to have a lasting impact on the field, as not only did subsequent sleep screening efforts uncover the novel SHAKER-regulator *sleepless*, (Koh et al., 2009), but investigations into SHAKER's beta subunit HYPERKINETIC ultimately revealed a critical role for this redox sensor linking metabolic function to sleep (Bushey et al., 2007; Kempf et al., 2019). Other *Drosophila* loss of function screens have highlighted the sleep-regulatory roles of the dopamine transporter, *fumin*, (Wu et al., 2008) and the Cullin-3 ubiquitin ligase adaptor, *insomniac* (Pfeiffenberger and Allada, 2012; Stavropoulos and Young, 2011), among others.

Disparate screening strategies across model organisms continue to unveil novel sleep modulators in both invertebrate and vertebrate model systems. For example, the roles of RFamide receptor DMSR-1 in stress-induced sleep in *C. elegans* (Iannacone et al., 2017) and SIK3 kinase in modulating sleep homeostasis in mice (Funato et al., 2016) were identified in genetic screens. Moreover, a gain of function screening strategy in *Drosophila* revealed the novel sleep and immune regulator, *nemuri* (Toda et al., 2019), and a zebrafish overexpression screen uncovered the secreted neuropeptides Neuromedin U and Neuropeptide Y, which decrease and increase sleep, respectively (Chiu et al., 2016; Singh et al., 2017). The continued success of screening strategies in revealing novel sleep-wake regulatory genes suggests that more sleep signals likely remain to be discovered.

One of the lessons from these genetic screens is that many of the uncovered genes play conserved roles across species—for example, Shaker also regulates mammalian sleep (Douglas et al., 2007) and RFamides induce sleep in worms, flies, and vertebrates (Lee et al.,

2017; Lenz et al., 2015). Nevertheless, not every invertebrate sleep-regulatory gene has a clear homolog in vertebrate species, while known human sleep/wake regulators, such as the narcolepsy-associated neuropeptide hypocretin/orexin and its receptors, lack invertebrate orthologs (Chemelli et al., 1999; Lin et al., 1999; Prober et al., 2006; Sakurai, 2013; Yokogawa et al., 2007). Therefore, genetic sleep screens in vertebrates are likely to provide added value in uncovering additional regulatory components required to control the initiation and amount of sleep.

While sleep screening in mammals is feasible (Funato et al., 2016), it remains an expensive and technically challenging endeavour. With its genetic tractability, availability of high-throughput sleep assays (Rihel and Schier, 2013), and conserved sleep genetics, such as the hypocretin, melatonin, and raphe systems (Gandhi et al., 2015; Oikonomou et al., 2019; Prober et al., 2006), the larval zebrafish offers an attractive alternative vertebrate system for sleep screens. We took advantage of a collection of zebrafish lines that harbour viral-insertions in >3500 genes (Varshney et al., 2013) to perform a targeted genetic screen. We found one short-sleeping mutant, *dreammist*, with a disrupted novel, highly conserved, vertebrate gene that encodes a small single pass transmembrane protein. Sequence and structural homology to the Na^+/K^+ pump regulator FXYD1/Phospholemman suggests that Dreammist is a neuronal-expressed member of a class of sodium pump modulators that is important for regulating sleep-wake behaviour.

RESULTS

Reverse genetic screen identifies *dreammist,* a mutant with decreased sleep

We used the availability of the 'Zenemark' viral-insertion based zebrafish gene knock-out resource (Varshney et al., 2013) to perform a reverse genetic screen to identify novel vertebrate sleep genes. This screening strategy offers several advantages compared to traditional chemical mutagenesis-based forward genetic screening approaches. First, unlike chemical mutagenesis, which introduces mutations randomly, viral insertions tend to target the 5' end of genes, typically causing genetic loss of function (Sivasubbu et al., 2007). Second, because the virus sequence is known, it is straightforward to map and identify the causative gene in mutant animals. Finally, since viral insertions in the Zenemark collection are already mapped and sequenced, animals harbouring insertions within specific gene classes can be selected for testing (Figure S1A). This allowed us to prioritise screening of genes encoding protein classes most often linked to behaviour, such as G-protein coupled receptors, neuropeptide ligands, and ion channels and transporters (Supplemental Data 1).

For screening, we identified zebrafish sperm samples from the Zenemark collection (Varshney et al., 2013) that harboured viral insertions in genes of interest and used these samples for *in vitro* fertilization and the establishment of F2 families. For each viral insertion line, clutches from heterozygous F2 in-crosses were raised to 5 days post-fertilisation (dpf) and tracked using videography (Figure S1A) to quantify the number and duration of sleep bouts and the average waking activity (time spent moving per one-minute active bouts) over 48 hours. The genotypes of individual larvae were determined by PCR after behavioural tracking, with each larva assigned as wild type, heterozygous, or homozygous for a given viral insertion to assess the effect of genotype on sleep/wake behaviour. While most lines screened had minimal effects on sleep-wake behavioural parameters (Figure S1B-C), one homozygous viral insertion line, *10543/10543,* had a reduction in daytime sleep (Figure S1B) and an increase in daytime

waking activity (Figure S1C) relative to their wild type sibling controls. We re-named this *10543* viral insertion line *dreammist* (*dmist*).

In follow-up studies, we observed that animals homozygous for the viral insertion at this locus (*dmist*$^{vir/vir}$) showed a prominent decrease in sleep during the day and a trend to sleep less at night compared to their wild-type siblings (*dmist*$^{+/+}$) (Figure 1A). There was an almost 50% reduction in average daytime sleep (Figure 1C) due to a decrease in the number of sleep bouts (Figure 1D), and sleep bout length at night was significantly reduced (Figure 1E). *dmist*$^{vir/vir}$ larvae also exhibited significantly increased daytime waking activity (Figure 1B, F). Because Zenemark lines can contain more than one viral insertion (17.6% of lines have >=2 insertions; Varshney et al 2013), we outcrossed *dmist*$^{vir/+}$ fish to wild-type fish of the AB-TL background and re-tested *dmist* mutant fish over several generations. Normalising all the behavioural parameters to *dmist*$^{+/+}$ controls with a linear mixed effects (LME) model showed consistent sleep changes in *dmist*$^{vir/vir}$ fish over N=5 experiments. The *dmist*$^{vir/vir}$ larvae consistently show a more than 50% decrease in sleep during the day due to a significant reduction in the number and duration of sleep bouts, as well as a strong increase in waking activity (Figure 1G). The *dmist*$^{vir/vir}$ mutants also had a significant reduction in sleep at night compared to wild type siblings (Figure 1G). These effects on sleep and wakefulness are not due to alterations in circadian rhythms, as behavioural period length in fish that were entrained and then shifted to free-running constant dark conditions was unaffected in *dmist*$^{vir/vir}$ compared to wild-type sibling larvae (Figure S2A-C).

The *dmist* gene encodes a novel, small transmembrane protein

Having identified a sleep mutant, we next sought to investigate the target gene disrupted by the viral insertion. Line *10543* (*dmist*^{vir}) was initially selected for screening due to a predicted disruption of a gene encoding a serotonin transporter (*slc6a4b*) on chromosome 5. However,

mapping of the *dmist* viral insertion site by inverse-PCR and sequencing revealed that the virus was instead inserted into the intron of a small two-exon gene originally annotated in the Zv6 genome assembly as a long intergenic non-coding RNA (lincRNA; gene transcript ENSDART00000148146, gene name *si:dkey234h16.7*), which lies approximately 6 kilobases (kb) downstream of the *slc6a4b* gene in zebrafish. At least part of this region is syntenic across vertebrates, with a small two-exon gene consistently identified adjacent to the genes *ankrd13a* and *GIT* in several vertebrates, including human and mouse (Figure 2A). Amplifying both 5' and 3' ends of zebrafish *si:dkey234h16.7* and mouse E13.5 *1500011B03-001* transcripts with Rapid Amplification of cDNA ends (RACE) confirmed the annotated zebrafish and mouse transcripts and identified two variants with 3' untranslated regions (3'UTR) of different lengths in zebrafish (Figure S3B). To test whether the viral insertion in *dmist*$^{vir/vir}$ disrupts expression of *si:dkey234h16.7* or neighbouring genes, we performed quantitative analysis of gene transcript levels in wild type and mutant *dmist* larvae by RT-qPCR. This revealed that the *dmist* viral insertion caused a more than 70% knockdown in the expression of *si:dkey234h16.7* while the expression of the most proximal 5' or 3' flanking genes, *slc6a4b_Dr* and *ankrd13a_Dr*, were unaffected (Figure 2B, Figure S3A). Since this disruption of expression is most consistent with *si:dkey234h16.7* being the causal lesion of the *dmist* mutant sleep phenotype, we renamed this gene *dreammist* (*dmist*).

Although originally annotated as a lincRNA, computational predictions indicated that the *dmist* transcripts contain a small open reading frame (ORF) encoding a protein of 70 amino acids (aa) (Figure 2C, Figure S3B). Furthermore, mining of ribosome profiling datasets in zebrafish has shown that *dmist* is found in polyribosomes (Chew et al., 2013), and chromatin immunoprecipitation sequencing data (Pauli et al., 2015; Ulitsky et al., 2011) had identified that the locus contains histone methylation states associated with protein-coding genes (Aday et al., 2011). Incorporating this evidence, updated zebrafish genome assemblies (Zv9-11) have

annotated *dmist* as a small protein-coding gene. Querying the human and vertebrate protein databases by BLASTp using the C-terminal protein sequence of Dmist identified orthologs in most other vertebrate clades, including other species of teleost fish, birds, amphibians, and mammals (Figure 2A, C). All identified orthologs encoded predicted proteins with an N-terminal signal peptide sequence and a C-terminal transmembrane domain (Figure 2C). The peptide sequence identity across orthologs ranged from 38 to 84%, with three peptide motifs (QNLV, CVYKP, RRR) showing high conservation across all vertebrates (Figure 2C, Figure S3D). In summary, we found that the *dreammist* gene, the expression of which is disrupted in *dmist*$^{vir/vir}$ fish with sleep phenotypes, encodes a protein that is highly conserved across vertebrates at both the genomic and molecular levels.

Genetic molecular analysis of *dmist* expression in zebrafish and mouse

Because the viral insertion disrupts *dmist* throughout the animal's lifetime, we examined both the developmental and spatial expression of *dmist* to assess when and where its function may be required for proper larval sleep. Using the full-length transcript as a probe (Figure S3B), we performed *in situ* hybridization across embryonic and larval development. Maternally deposited *dmist* was detected in early embryos (2-cell stage) prior to the maternal to zygotic transition (Giraldez et al., 2006) (Figure 2D). Consistent with maternal deposition of *dmist* transcripts, inspection of the 3' end of the *dmist* gene revealed a cytoplasmic polyadenylation element ('TTTTTTAT'; Supplemental Information 2) that is required for zygotic translation of maternal transcripts (Villalba et al., 2011). At 24hpf, transcripts were detected in regions that form the embryonic brain, such as ventral telencephalon, diencephalon and cerebellum, and in the developing eye (Figure 2D, S3C). By 5dpf, *dmist* transcripts were detected throughout the brain (Figure 2D). To test whether *dmist* transcripts are under circadian regulation, we performed RT-qPCR in fish that were entrained and then shifted to free-running constant dark

conditions. In contrast with the robust 24-hr rhythmic transcription of the circadian clock gene *per1*, we did not detect any changes in *dmist* expression throughout the 24 hour circadian cycle (Figure S2D).

Consistent with brain expression in larval zebrafish, we identified the expression of *Dmist_Mm* in a published RNAseq dataset of six isolated cell types from mouse cortex (Zhang et al., 2014). We confirmed that *Dmist_Mm* is specifically enriched in neurons by hierarchical clustering of all 16,991 expressed transcripts across all six cells types, which demonstrated that *Dmist_Mm* co-clusters with neuronal genes (Figure S3E). Pearson correlation of *Dmist_Mm* with canonical markers for the six cell types showed that *Dmist_Mm* expression is highly correlated with other neuronal genes but not genes associated with microglia, oligodendrocytes, or endothelia. This indicates that *dmist* is specifically expressed in neurons in both zebrafish and mouse (Figure S3F).

Dmist localises to the plasma membrane

Although the *dreammist* gene encodes a conserved ORF with a predicted signal peptide sequence and transmembrane domain (Figure 2C; Figure S3G-I), we wanted to confirm this small peptide can localise to the membrane and if so, on which cellular compartments. To test these computational predictions, we transiently co-expressed GFP-tagged Dmist (C-terminal fusion) with a marker for the plasma membrane (myr-Cherry) in zebrafish embryos. Imaging at 90% epiboly revealed Dmist-GFP localised to the plasma membrane (Figure 2E). Conversely, introducing a point mutation into Dmist's signal peptide cleavage site (DmistA22W-GFP) prevented Dmist from trafficking to the plasma membrane, with likely retention in the endoplasmic reticulum (Figure 2F). Together, these data indicate that Dmist localises to the plasma membrane despite its small size, as computationally predicted.

CRISPR/Cas9 generated *dmist^{i8}* mutant exhibits decreased night-time sleep

The original viral insertion line had reduced *dmist* expression by 70%, suggesting that *dmist^{vir}* is a hypomorphic allele. To confirm that the sleep phenotypes observed in *dmist$^{vir/vir}$* animals are due to the disruption of Dmist function, we used CRISPR/Cas9 to create an independent *dmist* loss of function allele. We generated a zebrafish line in which the *dmist* gene contains an 8bp insertion that causes a frameshift and early stop (*dmist^{i8}*, Figure 3A). The *dmist^{i8}* allele is predicted to encode a truncated protein lacking the complete signal peptide sequence and transmembrane domain (Figure 3B), indicating this is likely a null allele. RT-qPCR showed that *dmist* transcript levels were 60% lower in *dmist$^{i8/i8}$* fish compared to wild type siblings, consistent with nonsense-mediated decay (Figure S4A, B).

We next assessed the sleep and activity patterns of *dmist$^{i8/i8}$* fish. As seen in exemplar individual tracking experiments, *dmist$^{i8/i8}$* larvae sleep less at night due to fewer sleep bouts as well as an increase in waking activity relative to wild type and heterozygous mutant siblings (Figure 3C-H). This significant night-time reduction in sleep and increase in wakefulness is also apparent when combining N=5 independent experiments with an LME model to normalize behaviour across datasets (Figure 3I). Although *dmist$^{vir/vir}$* larvae also slept less at night (Figure 1G), the large day-time reduction in sleep observed in *dmist$^{vir/vir}$* larvae is absent in *dmist$^{i8/i8}$* animals, perhaps because of differences in the *dmist^{vir}* genetic background affecting behaviour. In addition, because the *dmist^{vir}* is likely a hypomorphic allele, we focused subsequent experiments on the CRISPR-generated *dmist$^{i8/i8}$* larvae.

To test whether the increased night-time activity of *dmist$^{i8/i8}$* mutants persists in older animals, we raised *dmist$^{i8/i8}$* mutants with their heterozygous and wild type siblings to adulthood in the same tank and tracked individual behaviour for several days on a 14:10 light:dark cycle. As in larval stages, *dmist$^{i8/i8}$* adults were hyperactive relative to both *dmist$^{i8/+}$* and *dmist$^{+/+}$*

siblings, maintaining a higher mean speed at night (Figure 3L-M, S4D). This suggests that either Dmist affects a sleep/wake regulatory circuit during development that is permanently altered in *dmist* mutants or that Dmist is continuously required to maintain normal levels of night-time locomotor activity.

***dmist* mutants have altered sleep homeostasis**

The timing and duration of sleep is regulated by both circadian and homeostatic processes (Borbély, 1982). Since the disruption of *dmist* does not affect circadian regulation of sleep (Figure S2A-C), we tested whether *dmist* mutants have deficits in sleep homeostasis.

We have previously shown in zebrafish that a brief exposure to hyperactivity-inducing drugs such as the epileptogenic pentylenetetrazol (PTZ) or wake-promoting caffeine induces a dose-dependent increase in homeostatic rebound sleep following drug washout that is phenotypically and mechanistically similar to rebound sleep following physical sleep deprivation (Reichert et al., 2019). Upon wash-on/wash-off of 5mM PTZ, sleep rebound occurs in approximately 50% of wild type larvae (Reichert et al., 2019; Figure 3K). In contrast, all $dmist^{i8/i8}$ larvae showed increased rebound sleep compared to $dmist^{+/+}$ sibling controls (Figure 3J, K, Figure S4C). Such sensitivity to sleep pressure induced by neuronal activity suggests that $dmist^{i8/i8}$ fish either have accumulated high basal levels of sleep pressure, for example as a consequence of extended wakefulness at night, or more rapidly accumulate sleep pressure in response to increased brain activity during waking. This result indicates that $dmist^{i8/i8}$ fish have disrupted sleep homeostasis.

In summary, long-term tracking across both *dmist* alleles and assessment of responses to drug-induced sleep pressure indicates that Dmist is a sensitive modulator of sleep/wake states.

Dmist is distantly related to the Na^+/K^+ pump regulator Fxyd1 (Phospholemman)

Because Dmist is a small, single pass transmembrane domain protein without any clear functional motifs, we searched for similar peptides that might provide clues for how Dmist might regulate behaviour. Using the multiple sequence alignment tool MAFFT to align the zebrafish, mouse, and human Dmist peptides (Katoh and Toh, 2010) and seeding a JackHMMR iterative search of the Uniprot database (Johnson et al., 2010) found distant homology between Dmist and Fxyd1/Phospholemman (Figure 4A), a small transmembrane domain peptide that regulates ion channels and pumps, including the Na^+,K^+-ATPase pump (Crambert et al., 2002). Dmist and Fxyd1 share 27-34% amino acid homology, including an RRR motif at the C-terminal end, although Dmist lacks a canonical FXYD domain (Figure 4A). This similarity suggested that Dmist may belong to a class of small, single pass transmembrane ion pump regulators.

Using *In situ* hybridisation, we found that *fxyd1* is expressed in cells along the brain ventricle and choroid plexus (Figure 4C) in contrast to the neuronal expression of *dmist* (Figure 2D). Despite these different expression patterns, based on their sequence similarity we reasoned that Fxyd1 and Dmist may regulate the same molecular processes that are involved in sleep. To test this hypothesis, we used CRISPR/Cas9 to generate a 28 bp deletion in the 3rd exon of the zebrafish *fxyd1* gene, causing a frameshift and severely truncated protein that lacks the FXYD, transmembrane, and C-terminal domains (Figure 4B). Contrary to a previous report based on morpholino knockdown (Chang et al., 2012), *fxyd1*$^{\Delta 28/\Delta 28}$ larvae were viable with no detectable defect in inflation of the brain ventricles. We therefore tested *fxyd1* mutant larvae for sleep phenotypes. Like *dmist* mutants, *fxyd1*$^{\Delta 28/\Delta 28}$ larvae slept less at night (Figure 4D-F). Interestingly, this sleep loss is mainly due to shorter sleep bouts (Figure 4F), indicating that *fxyd1* mutants initiate sleep normally but do not properly maintain it, unlike *dmist* mutants, which initiate fewer night-time sleep bouts, although in both cases there is consolidation of the

waking state at night (Figure 3I). Thus, despite the non-neuronal expression of *fxyd1* in the brain, the gene most closely related to *dmist* also modulates sleep at night.

The brain-wide Na^+/K^+ pump alpha subunit Atp1a3a regulates sleep at night

Given the similarity between Dmist and Fxyd1 and their effects on night-time sleep, we hypothesized that mutations in Na^+/K^+ pump subunits known to interact with Fxyd1 might also affect sleep. We focused on the Na^+/K^+ pump alpha-3 subunit (Atp1a3), as this has been shown to directly interact with Fxyd1 in mammalian brain tissue (Feschenko et al., 2003) and mutations in *ATP1A3* in humans causes several neurological and movement disorders, including rapid-onset dystonia parkinsonism (De Carvalho Aguiar et al., 2004) and alternating hemiplegia of childhood (Heinzen et al., 2014, 2012). Murine *Dmist* expression correlates well with *Atp1a3* distribution across 5 brain cell types in mouse (Pearson correlation coefficient = 0.63). Zebrafish have two Atp1a3 paralogs, *atp1a3a* and *atp1a3b*. Similar to *dmist*, *atp1a3a* is widely expressed in the larval zebrafish brain (Figure 5C, compare to Figure 2D). While *atp1a3b* is also expressed in the zebrafish brain, its expression is more limited to regions of the midbrain and hindbrain (Figure 5C). To test whether these subunits are involved in regulating zebrafish sleep, we made CRISPR-targeted mutants of both *atp1a3a* and *atp1a3b* and isolated an allele with a 19 base deletion in *atp1a3a* and an allele with a 14 base deletion in *atp1a3b*. Both mutations are predicted to generate null alleles due to deletion of the start codon (Figure 5A, B). Both $atp1a3a^{\Delta 19/\Delta 19}$ and $atp1a3b^{\Delta 14/\Delta 14}$ mutant larvae were healthy and viable through early development, and, contrary to a previous report based on morpholino injections (Doğanli et al., 2013), neither mutant had defects in the inflation of their brain ventricles. Sleep-wake tracking experiments found that $atp1a3b^{\Delta 14/\Delta 14}$ mutants were slightly more active during the day but did not have sleep phenotypes (Figure 5F, G). In contrast, mutation of *atp1a3a* resulted in large effects on sleep-wake behaviour. Compared to wild type

316 and heterozygous siblings, *atp1a3a*$^{\Delta 19/\Delta 19}$ mutants were hyperactive throughout the day and
317 night, and had a large reduction in sleep at night (Figure 5D, F). The night-time sleep reduction
318 was due to a reduction in the length of sleep bouts, as *atp1a3a* mutants even had a small
319 increase in the number of sleep bouts at night (Figure 5F).

320 The similar night-time reduction in sleep in *dmist* and *atp1a3a* mutants, combined with the
321 protein homology between Dmist and Fxyd1, suggested that Dmist may be involved in
322 regulating the Na^+/K^+ pump. Consistent with this hypothesis, brains from both *dmist*$^{i8/i8}$ and
323 *atp1a3a*$^{\Delta 19/\Delta 19}$ larvae had elevated intracellular sodium levels after exposure to PTZ (Figure
324 5G). Thus, neither *dmist* nor *atp1a3a* mutants were able to restore intracellular sodium balance
325 after sustained neuronal activity as quickly as wild type siblings. Consistent with the night-
326 specific alterations in sleep behaviour, we also found that baseline brain Na^+ levels in *dmist*
327 mutants were significantly elevated at night but not during the day (Figure 5H). Collectively,
328 these data are consistent with the hypothesis that night-time sleep duration is affected by
329 changes in Na^+/K^+ pump function and that Dmist is required for maintaining this function both
330 at night and after sustained neuronal activity.

DISCUSSION

Genetic screening discovers *dmist*, a novel sleep-regulatory gene

Using a reverse genetic viral screening strategy, we discovered a short-sleeping mutant, *dmist*, which has a disruption in a previously uncharacterized gene encoding a small transmembrane peptide. Given that the *dmist* mutant appeared within the limited number of lines that we screened, it is likely that many other sleep genes are still waiting to be discovered in future screens. In zebrafish, one promising screening strategy will be to employ CRISPR/Cas9 genome editing to systematically target candidate genes. Advances in the efficiency of this technology now makes it feasible to perform a CRISPR "F0 screen" in which the consequences of bi-allelic, gene-specific mutations are rapidly tested in the first generation, with only the most promising lines pursued in germline-transmitted mutant lines (Grunwald et al., 2019; Jao et al., 2013; Shah et al., 2015; Shankaran et al., 2017; Wu et al., 2018). CRISPR F0 screens could be scaled to systematically target the large number of candidate sleep-regulatory genes identified through human GWAS studies and sequencing of human patients suffering from insomnia and neuropsychiatric disorders (Allebrandt et al., 2013; Jansen et al., 2019; Lek et al., 2016; Palagini et al., 2019).

Dmist is related to the Na+/K+ pump regulator Fxyd1

The small Dmist transmembrane protein is highly conserved across vertebrates, expressed in neurons, and important for maintaining normal sleep levels. How can such a small, single pass transmembrane protein lacking any clear functional domains modulate the function of neurons and ultimately animal behaviour? The recognition that Dmist has sequence homology (~35% amino acid similarity) and structural homology (e.g. signal peptide and single pass transmembrane domains; a conserved 'RRR' motif) to the Na^+,K^+-ATPase pump regulator Fxyd1 (Phospholemman) offers some important clues.

Fxyd1/Phospholemman is a member of the FXYD protein family, of which there are seven mammalian members (Sweadner and Rael, 2000). Each of the FXYD proteins is small, contains a characteristic FXYD domain, and has a single transmembrane domain. FXYD family members interact with alpha subunits of the Na^+,K^+ ATPase to regulate the function of this pump, with individual family members expressed in different tissues to modulate Na+,K+ ATPase activity depending on the physiological needs of the tissue (Geering et al., 2003). In cardiac muscle, FXYD1 is thought to act as a hub through which various signalling cascades, such as PKA, PKC, or nitric oxide, can activate or inhibit Na^+ pump activity (Pavlovic et al., 2013). For example, FXYD1 is critical for mediating the increased Na^+ pump activity observed after β-receptor stimulation via cAMP-PKA signalling (Despa et al., 2008). Much less is known about FXYD1's role in non-cardiac tissue, although it is expressed in neurons in the mammalian cerebellum, the choroid plexus, and ependymal cells, where it interacts with all three alpha subunits of the Na^+,K^+ ATPase (Feschenko et al., 2003).

In zebrafish, we also found that *fxyd1* is expressed in cells around the ventricles and in the choroid plexus (Figure 4C), in contrast to *dmist* which is expressed in neurons throughout the brain. Despite the different expression patterns, mutation of each gene resulted in a similar reduction of sleep at night. However, unlike *dmist* mutants, which have fewer sleep bouts (i.e. initiate sleep less) and an increase in waking locomotor activity, *fxyd1* mutants have shorter sleep bouts (i.e. cannot maintain sleep) on average and do not have a locomotor activity phenotype. Just as the various FXYD family members modulate the Na^+/K^+ pump in different tissue- and context-specific ways, this phenotypic variation between *fxyd1* and *dmist* mutants could be due to the different *fxyd1* and *dmist* expression patterns, modulation kinetics of pump/channel dynamics, or interaction with alternative accessory proteins or signal transduction cascades. Nevertheless, the similar timing and magnitude of sleep reduction,

combined with the structural similarity of Fxyd1 and Dmist, suggest that they may regulate similar sleep-related processes.

Dmist, the sodium pump, and sleep

The similarity between Dmist and FXYD1 led us to directly manipulate the Na^+,K^+ ATPase to test its importance in sleep. The Na^+,K^+-ATPase is the major regulator of intracellular Na^+ in all cells and, by actively exchanging two imported K^+ ions for three exported Na^+ ions, is essential for determining cellular resting membrane potential (reviewed in Clausen et al., 2017). The Na^+,K^+-ATPase is made up of a catalytic alpha subunit (4 known isoforms, ATP1A1-4), a supporting beta subunit (3 isoforms, ATP1B1-3), and a regulatory gamma subunit (the FXYD proteins). The alpha1 and alpha3 subunits are the predominant catalytic subunits in neurons (alpha2 is mostly restricted to glia), although the alpha1 subunit is also used ubiquitously in all tissues (McGrail et al., 1991). By mutating zebrafish orthologs of *Atp1a3*, we therefore could test the neuronal-specific role of the Na^+,K^+-ATPase in sleep.

Mutations in both zebrafish *Atp1a3* orthologs increased waking locomotor behaviour during the day. However, only mutations in the brain-wide *atp1a3a,* but not in the more restricted *atp1a3b*, led to changes in night-time sleep. The *atp1a3a* mutants have a bigger sleep reduction than either $dmist^{vir}$, $dmist^{i8}$ or $fxyd1^{\Delta 28}$ mutants, which is expected since increased phenotypic severity is a common feature of perturbations in ion channel/pump subunits compared to their modulators (Cirelli et al., 2005; Wu et al., 2014). Autosomal dominant missense mutations leading to loss of function in *ATP1A3* cause movement disorders such as rapid-onset dystonia parkinsonism and childhood alternating hemiplegia (recurrent paralysis on one side) in humans (Canfield et al., 2002; Heinzen et al., 2014), while loss of function mutations in *Atp1a3* result in generalised seizures and locomotor abnormalities, including

hyperactivity, in mice (Clapcote et al., 2009; Hunanyan et al., 2015; Ikeda et al., 2013; Kirshenbaum et al., 2011; Sugimoto et al., 2014). Our data also suggests that, in addition to movement abnormalities, insomnia at night is a direct behavioural consequence of *atp1a3a* mutation, consistent with a recent report of very high prevalence of insomnia in patients with childhood alternating hemiplegia, some of which harboured mutations in *Atp1a3* (Kansagra et al., 2019). Small molecule screens aimed at ameliorating zebrafish *atp1a3a* mutant phenotypes may therefore be a promising approach for the rapid identification of new therapies for the management of this disease (Hoffman et al., 2016; Rihel et al., 2010).

Together, the night-specific sleep phenotypes of *dmist*, *fxyd1*, and *atp1a3a* mutants point to a role for the Na^+,K^+-ATPase in boosting sleep at night. How might the alpha3 catalytic subunit of the Na^+/K^+ pump regulate sleep, and how could Dmist be involved? Compared to the alpha1 subunit, Atp1a3 has a lower affinity for Na^+ ions, and therefore plays an essential role in repolarizing neurons in response to rapid Na^+ increases during high levels of neuronal activity (Azarias et al., 2013). We confirmed that Atp1a3a is essential in zebrafish for re-establishing proper brain intracellular Na^+ levels following high neuronal activity induced by the GABA-receptor antagonist, PTZ. Dmist is also essential for re-establishing brain Na^+ levels after PTZ exposure (Figure 5G) but not during the baseline day conditions (Figure 5H). Given that the intensity of global neuronal activity impacts the magnitude of subsequent sleep rebound and engagement of the Galanin sleep-homeostatic output arm (Reichert et al., 2019), this model of Dmist-Atp1a3a rebalancing Na^+ during high neuronal firing can also explain the observed exaggerated sleep rebound in *dmist* mutants following a short PTZ exposure (Figure 3J) as a consequence of increased neuronal depolarization due to defective Na^+ pump activity. Intriguingly, a meta-analysis of neuronal transcripts that increase during rodent sleep deprivation found mouse *Dmist* among the top responding genes (Stuart Peirson, personal communication), suggesting Dmist may play a similar role in regulating neuronal responses to

physical sleep deprivation in mammals. Whether this transcriptional change reflects functional modulation of the Na^+/K^+ pump in mammalian neurons awaits experimental validation.

We also found that Dmist is required for proper maintenance of brain intracellular Na^+ levels selectively at night but not during the baseline day, mirroring the timing of sleep disruption in *dmist*$^{i8/i8}$ animals. This suggests that the decreased night-time sleep of *dmist* mutants is due to a specific requirement for Dmist modulation of the Na^+/K^+ pump at night. However, we cannot exclude the possibility that Dmist's function is required in only a subset of critical sleep/wake regulatory neurons during the day that then influence behaviour at night, such as the wake-active, sleep-homeostatic regulating serotonergic neurons of the dorsal raphe (Oikonomou et al., 2019). Another possibility is that disruption of proper establishment of the Na^+ electrochemical gradient in *dmist* mutant neurons leads to dysfunction of various neurotransmitter reuptake transporters, including those for glycine, GABA, glutamate, serotonin, dopamine, and norepinephrine, which rely on energy from the Na^+ gradient to function (Kristensen et al., 2011). A third possibility is that Dmist and the Na^+,K^+-ATPase regulate sleep not by modulation of neuronal activity per se but rather via modulation of extracellular ion concentrations. Recent work has demonstrated that interstitial ions fluctuate across the sleep/wake cycle in mouse; for example, extracellular K^+ is high during wakefulness (Ding et al., 2016). Moreover, cerebrospinal fluid containing the ion concentrations found during wakefulness directly applied to the brain can locally shift neuronal activity into wake-like states. Given that the Na^+,K^+-ATPase actively exchanges Na^+ ions for K^+ , the high intracellular Na^+ levels we observe in *atp1a3a* and *dmist* mutants is likely accompanied by high extracellular K^+. Although we can only speculate at this time, a model in which extracellular ions that accumulate during wakefulness and then directly signal onto sleep-regulatory neurons could provide a direct link between Na^+,K^+ ATPase activity, neuronal firing, and sleep homeostasis.

453 In conclusion, through a genetic screening strategy in zebrafish, we have identified a novel
454 brain expressed gene that encodes a small transmembrane protein regulator of night-time
455 sleep and wake behaviours. Future work will be required to uncover the precise signalling
456 dynamics by which Dmist regulates the Na^+,K^+-ATPase and sleep.

457 **Acknowledgements**

458 The initial screen, discovery, and characterization of *dreammist* was conducted in the lab of
459 Alexander F Schier at Harvard University. We also would like to thank members of the Rihel
460 lab and other UCL zebrafish groups for helpful comments on experiments and the manuscript
461 over the years. We thank Shannon Shibata-Germanos for *fxyd1* mutant tracking experiments,
462 John Parnavalas for reagents, Christine Orengo for help with small peptide sequence
463 searches, Stuart Peirson for early access to mouse transcriptomic data, and Finn Mango
464 Bamber for the Pokémon-card inspired *dreammist* name. The work was funded by grants
465 awarded to Alexander Schier, R01 GM085357 and HL10952505; an ERC Starting Grant
466 (#282027) and Wellcome Trust Investigator Award (#217150/Z/19/Z) to JR; National Institutes
467 of Health grant NS101158 to DAP; and a Grand Challenges PhD studentship to ILB.

468

469

REFERENCES

Aday, A.W., Zhu, L.J., Lakshmanan, A., Wang, J., and Lawson, N.D., 2011. Identification of cis regulatory features in the embryonic zebrafish genome through large-scale profiling of H3K4me1 and H3K4me3 binding sites. Dev. Biol. 357, 450–462. https://doi.org/10.1016/j.ydbio.2011.03.007

Allebrandt, K. V, Amin, N., Müller-Myhsok, B., Esko, T., Teder-Laving, M., Azevedo, R.V.D.M., Hayward, C., van Mill, J., Vogelzangs, N., Green, E.W., et al., 2013. A KATP channel gene effect on sleep duration: from genome-wide association studies to function in Drosophila. Mol. Psychiatry 18, 122–132. https://doi.org/10.1038/mp.2011.142

Azarias, G., Kruusmägi, M., Connor, S., Akkuratov, E.E., Liu, X.L., Lyons, D., Brismar, H., Broberger, C., and Aperia, A., 2013. A specific and essential role for Na,K-ATPase α3 in neurons co-expressing α1 and α3. J. Biol. Chem. 288, 2734–2743. https://doi.org/10.1074/jbc.M112.425785

Barlow, I.L., and Rihel, J., 2017. Zebrafish sleep: from geneZZZ to neuronZZZ. Curr. Opin. Neurobiol. 44, 65–71. https://doi.org/10.1016/j.conb.2017.02.009

Borbély, A.A., 1982. A two process model of sleep regulation. Hum. Neurobiol.

Bushey, D., Huber, R., Tononi, G., and Cirelli, C., 2007. Drosophila Hyperkinetic mutants have reduced sleep and impaired memory. J. Neurosci. 27, 5384–93. https://doi.org/10.1523/JNEUROSCI.0108-07.2007

Canfield, V.A., Loppin, B., Thisse, B., Thisse, C., Postlethwait, J.H., Mohideen, M.-A.P.., Rajarao, S.J.R., and Levenson, R., 2002. Na,K-ATPase α and β subunit genes exhibit unique expression patterns during zebrafish embryogenesis. Mech. Dev. 116, 51–59. https://doi.org/10.1016/S0925-4773(02)00135-1

Chang, J.T., Lowery, L.A., and Sive, H., 2012. Multiple roles for the Na,K-ATPase subunits,

494 Atp1a1 and Fxyd1, during brain ventricle development. Dev. Biol. 368, 312–22.
495 https://doi.org/10.1016/j.ydbio.2012.05.034

496 Chemelli, R.M., Willie, J.T., Sinton, C.M., Elmquist, J.K., Scammell, T., Lee, C., Richardson,
497 J.A., Clay Williams, S., Xiong, Y., Kisanuki, Y., et al., 1999. Narcolepsy in orexin
498 knockout mice: Molecular genetics of sleep regulation. Cell 98, 437–451.
499 https://doi.org/10.1016/S0092-8674(00)81973-X

500 Chew, G.-L., Pauli, A., Rinn, J.L., Regev, A., Schier, A.F., and Valen, E., 2013. Ribosome
501 profiling reveals resemblance between long non-coding RNAs and 5' leaders of coding
502 RNAs. Development 140, 2828–34. https://doi.org/10.1242/dev.098343

503 Chiu, C.N., Rihel, J., Lee, D.A., Singh, C., Mosser, E.A., Chen, S., Sapin, V., Pham, U.,
504 Engle, J., Niles, B.J., et al., 2016. A Zebrafish Genetic Screen Identifies Neuromedin U
505 as a Regulator of Sleep/Wake States. Neuron 89, 842–856.
506 https://doi.org/10.1016/j.neuron.2016.01.007

507 Cirelli, C., 2009. The genetic and molecular regulation of sleep: from fruit flies to humans.
508 Nat. Rev. Neurosci. 10, 549–60. https://doi.org/10.1038/nrn2683

509 Cirelli, C., Bushey, D., Hill, S., Huber, R., Kreber, R., Ganetzky, B., and Tononi, G., 2005.
510 Reduced sleep in Drosophila Shaker mutants. Nature 434, 1087–1092.
511 https://doi.org/10.1038/nature03486

512 Clapcote, S.J., Duffy, S., Xie, G., Kirshenbaum, G., Bechard, A.R., Schack, V.R., Petersen,
513 J., Sinai, L., Saab, B.J., Lerch, J.P., et al., 2009. Mutation I810N in the α3 isoform of
514 Na+,K +-ATPase causes impairments in the sodium pump and hyperexcitability in the
515 CNS. Proc. Natl. Acad. Sci. U. S. A. 106, 14085–14090.
516 https://doi.org/10.1073/pnas.0904817106

517 Clausen, M. V, Hilbers, F., and Poulsen, H., 2017. The Structure and Function of the Na,K-

518 ATPase Isoforms in Health and Disease. Front. Physiol. 8, 371.
519 https://doi.org/10.3389/fphys.2017.00371

520 Crambert, G., Fuzesi, M., Garty, H., Karlish, S., and Geering, K., 2002. Phospholemman
521 (FXYD1) associates with Na,K-ATPase and regulates its transport properties. Proc. Natl.
522 Acad. Sci. U. S. A. 99, 11476–81. https://doi.org/10.1073/pnas.182267299

523 De Carvalho Aguiar, P., Sweadner, K.J., Penniston, J.T., Zaremba, J., Liu, L., Caton, M.,
524 Linazasoro, G., Borg, M., Tijssen, M.A.J., Bressman, S.B., et al., 2004. Mutations in the
525 Na+/K+-ATPase α3 gene ATP1A3 are associated with rapid-onset dystonia
526 parkinsonism. Neuron 43, 169–175. https://doi.org/10.1016/j.neuron.2004.06.028

527 Despa, S., Tucker, A.L., and Bers, D.M., 2008. Phospholemman-mediated activation of Na/K-
528 ATPase limits [Na]i and inotropic state during β-adrenergic stimulation in mouse
529 ventricular myocytes. Circulation 117, 1849–1855.
530 https://doi.org/10.1161/CIRCULATIONAHA.107.754051

531 Ding, F., O'donnell, J., Xu, Q., Kang, N., Goldman, N., and Nedergaard, M., 2016. Changes
532 in the composition of brain interstitial ions control the sleep-wake cycle. Science (80-.).
533 352, 550–555. https://doi.org/10.1126/science.aad4821

534 Doğanli, C., Beck, H.C., Ribera, A.B., Oxvig, C., and Lykke-Hartmann, K., 2013. α3Na+/K+-
535 ATPase deficiency causes brain ventricle dilation and abrupt embryonic motility in
536 zebrafish. J. Biol. Chem. 288, 8862–8874. https://doi.org/10.1074/jbc.M112.421529

537 Douglas, C.L., Vyazovskiy, V., Southard, T., Chiu, S.-Y., Messing, A., Tononi, G., and Cirelli,
538 C., 2007. Sleep in Kcna2 knockout mice. BMC Biol. 5, 42. https://doi.org/10.1186/1741-
539 7007-5-42

540 Feschenko, M.S., Donnet, C., Wetzel, R.K., Asinovski, N.K., Jones, L.R., and Sweadner,
541 K.J., 2003. Phospholemman, a single-span membrane protein, is an accessory protein

of Na,K-ATPase in cerebellum and choroid plexus. J. Neurosci. 23, 2161–2169. https://doi.org/10.1523/jneurosci.23-06-02161.2003

Funato, H., Miyoshi, C., Fujiyama, T., Kanda, T., Sato, M., Wang, Z., Ma, J., Nakane, S., Tomita, J., Ikkyu, A., et al., 2016. Forward-genetics analysis of sleep in randomly mutagenized mice. Nature 539, 378–383. https://doi.org/10.1038/nature20142

Gagnon, J.A., Valen, E., Thyme, S.B., Huang, P., Ahkmetova, L., Pauli, A., Montague, T.G., Zimmerman, S., Richter, C., and Schier, A.F., 2014. Efficient Mutagenesis by Cas9 Protein-Mediated Oligonucleotide Insertion and Large-Scale Assessment of Single-Guide RNAs. PLoS One 9, e98186. https://doi.org/10.1371/journal.pone.0098186

Gandhi, A. V, Mosser, E.A., Oikonomou, G., and Prober, D.A., 2015. Melatonin Is Required for the Circadian Regulation of Sleep. Neuron 85, 1–7. https://doi.org/10.1016/j.neuron.2015.02.016

Geering, K., Béguin, P., Garty, H., Karlish, S., Füzesi, M., Horisberger, J.D., and Crambert, G., 2003. FXYD proteins: New tissue- and isoform-specific regulators of Na,K-ATPase, in: Annals of the New York Academy of Sciences. New York Academy of Sciences, pp. 388–394. https://doi.org/10.1111/j.1749-6632.2003.tb07219.x

Giraldez, A.J., Mishima, Y., Rihel, J., Grocock, R.J., Van Dongen, S., Inoue, K., Enright, A.J., and Schier, A.F., 2006. Zebrafish MiR-430 promotes deadenylation and clearance of maternal mRNAs. Science 312, 75–79. https://doi.org/10.1126/science.1122689

Grunwald, H.A., Gantz, V.M., Poplawski, G., Xu, X.R.S., Bier, E., and Cooper, K.L., 2019. Super-Mendelian inheritance mediated by CRISPR–Cas9 in the female mouse germline. Nature. https://doi.org/10.1038/s41586-019-0875-2

Heinzen, E.L., Arzimanoglou, A., Brashear, A., Clapcote, S.J., Gurrieri, F., Goldstein, D.B., Jóhannesson, S.H., Mikati, M.A., Neville, B., Nicole, S., et al., 2014. Distinct neurological

disorders with ATP1A3 mutations. Lancet. Neurol. 13, 503–14. https://doi.org/10.1016/S1474-4422(14)70011-0

Heinzen, E.L., Swoboda, K.J., Hitomi, Y., Gurrieri, F., De Vries, B., Tiziano, F.D., Fontaine, B., Walley, N.M., Heavin, S., Panagiotakaki, E., et al., 2012. De novo mutations in ATP1A3 cause alternating hemiplegia of childhood. Nat. Genet. 44, 1030–1034. https://doi.org/10.1038/ng.2358

Hoffman, E.J., Turner, K.J., Fernandez, J.M., Cifuentes, D., Ghosh, M., Ijaz, S., Jain, R.A., Kubo, F., Bill, B.R., Baier, H., et al., 2016. Estrogens Suppress a Behavioral Phenotype in Zebrafish Mutants of the Autism Risk Gene, CNTNAP2. Neuron 89, 725–733. https://doi.org/10.1016/j.neuron.2015.12.039

Hunanyan, A.S., Fainberg, N.A., Linabarger, M., Arehart, E., Leonard, A.S., Adil, S.M., Helseth, A.R., Swearingen, A.K., Forbes, S.L., Rodriguiz, R.M., et al., 2015. Knock-in mouse model of alternating hemiplegia of childhood: Behavioral and electrophysiologic characterization. Epilepsia 56, 82–93. https://doi.org/10.1111/epi.12878

Iannacone, M.J., Beets, I., Lopes, L.E., Churgin, M.A., Fang-Yen, C., Nelson, M.D., Schoofs, L., and Raizen, D.M., 2017. The RFamide receptor DMSR-1 regulates stress-induced sleep in C. elegans. Elife 6. https://doi.org/10.7554/eLife.19837

Ikeda, K., Satake, S., Onaka, T., Sugimoto, H., Takeda, N., Imoto, K., and Kawakami, K., 2013. Enhanced inhibitory neurotransmission in the cerebellar cortex of Atp1a3-deficient heterozygous mice. J. Physiol. 591, 3433–3449. https://doi.org/10.1113/jphysiol.2012.247817

Jansen, P.R., Watanabe, K., Stringer, S., Skene, N., Bryois, J., Hammerschlag, A.R., de Leeuw, C.A., Benjamins, J.S., Muñoz-Manchado, A.B., Nagel, M., et al., 2019. Genome-wide analysis of insomnia in 1,331,010 individuals identifies new risk loci and functional

590 pathways. Nat. Genet. 51, 394–403. https://doi.org/10.1038/s41588-018-0333-3

591 Jao, L.-E., Wente, S.R., and Chen, W., 2013. Efficient multiplex biallelic zebrafish genome
592 editing using a CRISPR nuclease system. Proc. Natl. Acad. Sci. U. S. A. 110, 13904–9.
593 https://doi.org/10.1073/pnas.1308335110

594 Johnson, L.S., Eddy, S.R., and Portugaly, E., 2010. Hidden Markov model speed heuristic
595 and iterative HMM search procedure. BMC Bioinformatics 11, 431.
596 https://doi.org/10.1186/1471-2105-11-431

597 Joiner, W.J., 2016. Unraveling the Evolutionary Determinants of Sleep. Curr. Biol. 26,
598 R1073–R1087. https://doi.org/10.1016/j.cub.2016.08.068

599 Kansagra, S., Ghusayni, R., Kherallah, B., Gunduz, T., McLean, M., Prange, L., Kravitz,
600 R.M., and Mikati, M.A., 2019. Polysomnography findings and sleep disorders in children
601 with alternating hemiplegia of childhood. J. Clin. Sleep Med. 15, 65–70.
602 https://doi.org/10.5664/jcsm.7572

603 Katoh, K., and Toh, H., 2010. Parallelization of the MAFFT multiple sequence alignment
604 program. Bioinformatics. https://doi.org/10.1093/bioinformatics/btq224

605 Kempf, A., Song, S.M., Talbot, C.B., and Miesenböck, G., 2019. A potassium channel β-
606 subunit couples mitochondrial electron transport to sleep. Nature 568, 230–234.
607 https://doi.org/10.1038/s41586-019-1034-5

608 Kimmel, C.B., Ballard, W.W., Kimmel, S.R., Ullmann, B., and Schilling, T.F., 1995. Stages of
609 embryonic development of the zebrafish. Dev. Dyn. 203, 253–310.
610 https://doi.org/10.1002/aja.1002030302

611 Kirshenbaum, G.S., Clapcote, S.J., Duffy, S., Burgess, C.R., Petersen, J., Jarowek, K.J.,
612 Yücel, Y.H., Cortez, M.A., Snead, O.C., Vilsen, B., et al., 2011. Mania-like behavior
613 induced by genetic dysfunction of the neuron-specific Na+,K+-ATPase α3 sodium pump.

614 Proc. Natl. Acad. Sci. U. S. A. 108, 18144–18149.
615 https://doi.org/10.1073/pnas.1108416108

616 Koh, K., Joiner, W.J., Wu, M.N., Yue, Z., Smith, C.J., and Sehgal, A., 2009. Identification of
617 SLEEPLESS, a novel sleep promoting factor. Science (80-.). 321, 372–376.
618 https://doi.org/10.1126/science.1155942.Identification

619 Kristensen, A.S., Andersen, J., Jorgensen, T.N., Sorensen, L., Eriksen, J., Loland, C.J.,
620 Stromgaard, K., and Gether, U., 2011. SLC6 neurotransmitter transporters: Structure,
621 function, and regulation. Pharmacol. Rev. 63, 585–640.
622 https://doi.org/10.1124/pr.108.000869

623 Kwan, K.M., Fujimoto, E., Grabher, C., Mangum, B.D., Hardy, M.E., Campbell, D.S., Parant,
624 J.M., Yost, H.J., Kanki, J.P., and Chien, C.-B., 2007. The Tol2kit: a multisite gateway-
625 based construction kit for Tol2 transposon transgenesis constructs. Dev. Dyn. 236,
626 3088–99. https://doi.org/10.1002/dvdy.21343

627 Lee, D.A., Andreev, A., Truong, T. V., Chen, A., Hill, A.J., Oikonomou, G., Pham, U., Hong,
628 Y.K., Tran, S., Glass, L., et al., 2017. Genetic and neuronal regulation of sleep by
629 neuropeptide VF. Elife 6. https://doi.org/10.7554/eLife.25727

630 Lek, M., Karczewski, K.J., Minikel, E. V., Samocha, K.E., Banks, E., Fennell, T., O'Donnell-
631 Luria, A.H., Ware, J.S., Hill, A.J., Cummings, B.B., et al., 2016. Analysis of protein-
632 coding genetic variation in 60,706 humans. Nature 536, 285–291.
633 https://doi.org/10.1038/nature19057

634 Lenz, O., Xiong, J., Nelson, M.D., Raizen, D.M., and Williams, J.A., 2015. FMRFamide
635 signaling promotes stress-induced sleep in Drosophila. Brain. Behav. Immun. 47, 141–
636 148. https://doi.org/10.1016/j.bbi.2014.12.028

637 Lin, L., Faraco, J., Li, R., Kadotani, H., Rogers, W., Lin, X., Qiu, X., de Jong, P.J., Nishino, S.,

638 Mignot, E., et al., 1999. The sleep disorder canine narcolepsy is caused by a mutation in
639 the hypocretin (orexin) receptor 2 gene. Cell 98, 365–76. https://doi.org/10.1016/S0092-
640 8674(00)81965-0

641 Love, M.I., Huber, W., and Anders, S., 2014. Moderated estimation of fold change and
642 dispersion for RNA-seq data with DESeq2. Genome Biol. 15, 550.
643 https://doi.org/10.1186/s13059-014-0550-8

644 McGrail, K.M., Phillips, J.M., and Sweadner, K.J., 1991. Immunofluorescent localization of
645 three Na,K-ATPase isozymes in the rat central nervous system: Both neurons and glia
646 can express more than one Na,K-ATPase. J. Neurosci. 11, 381–391.
647 https://doi.org/10.1523/jneurosci.11-02-00381.1991

648 Montague, T.G., Cruz, J.M., Gagnon, J.A., Church, G.M., and Valen, E., 2014. CHOPCHOP:
649 a CRISPR/Cas9 and TALEN web tool for genome editing. Nucleic Acids Res. gku410-.
650 https://doi.org/10.1093/nar/gku410

651 Oikonomou, G., Altermatt, M., Zhang, R. wei, Coughlin, G.M., Montz, C., Gradinaru, V., and
652 Prober, D.A., 2019. The Serotonergic Raphe Promote Sleep in Zebrafish and Mice.
653 Neuron 103, 686-701.e8. https://doi.org/10.1016/j.neuron.2019.05.038

654 Palagini, L., Domschke, K., Benedetti, F., Foster, R.G., Wulff, K., and Riemann, D., 2019.
655 Developmental pathways towards mood disorders in adult life: Is there a role for sleep
656 disturbances? J. Affect. Disord. 243, 121–132.
657 https://doi.org/10.1016/J.JAD.2018.09.011

658 Pauli, A., Valen, E., Lin, M.F., Garber, M., Vastenhouw, N.L., Levin, J.Z., Fan, L., Sandelin,
659 A., Rinn, J.L., Regev, A., et al., 2012. Systematic identification of long noncoding RNAs
660 expressed during zebrafish embryogenesis Systematic identification of long noncoding
661 RNAs expressed during zebrafish embryogenesis 577–591.

https://doi.org/10.1101/gr.133009.111

Pauli, A., Valen, E., and Schier, A.F., 2015. Identifying (non-)coding RNAs and small peptides: Challenges and opportunities. BioEssays 37, 103–112. https://doi.org/10.1002/bies.201400103

Pavlovic, D., Fuller, W., and Shattock, M.J., 2013. Novel regulation of cardiac Na pump via phospholemman. J. Mol. Cell. Cardiol. 61, 83–93. https://doi.org/10.1016/j.yjmcc.2013.05.002

Pfeiffenberger, C., and Allada, R., 2012. Cul3 and the BTB Adaptor Insomniac Are Key Regulators of Sleep Homeostasis and a Dopamine Arousal Pathway in Drosophila. PLoS Genet. 8, e1003003. https://doi.org/10.1371/journal.pgen.1003003

Prober, D. a, Rihel, J., Onah, A. a, Sung, R.-J., and Schier, A.F., 2006. Hypocretin/orexin overexpression induces an insomnia-like phenotype in zebrafish. J. Neurosci. 26, 13400–10. https://doi.org/10.1523/JNEUROSCI.4332-06.2006

Reichert, S., Pavón Arocas, O., and Rihel, J., 2019. The Neuropeptide Galanin Is Required for Homeostatic Rebound Sleep following Increased Neuronal Activity. Neuron 104, 370-384.e5. https://doi.org/10.1016/j.neuron.2019.08.010

Rihel, J., Prober, D. a, Arvanites, A., Lam, K., Zimmerman, S., Jang, S., Haggarty, S.J., Kokel, D., Rubin, L.L., Peterson, R.T., et al., 2010. Zebrafish behavioral profiling links drugs to biological targets and rest/wake regulation. Science 327, 348–51. https://doi.org/10.1126/science.1183090

Rihel, J., and Schier, A.F., 2013. Sites of action of sleep and wake drugs: insights from model organisms. Curr. Opin. Neurobiol. 23, 831–40. https://doi.org/10.1016/j.conb.2013.04.010

Sakurai, T., 2013. Orexin deficiency and narcolepsy. Curr. Opin. Neurobiol. 23, 760–766.

https://doi.org/10.1016/j.conb.2013.04.007

Sehgal, A., and Mignot, E., 2011. Genetics of sleep and sleep disorders. Cell 146, 194–207. https://doi.org/10.1016/j.cell.2011.07.004

Shah, A.N., Davey, C.F., Whitebirch, A.C., Miller, A.C., and Moens, C.B., 2015. Rapid reverse genetic screening using CRISPR in zebrafish. Nat. Methods 12, 535–540. https://doi.org/10.1038/nmeth.3360

Shankaran, S.S., Dahlem, T.J., Bisgrove, B.W., Yost, H.J., and Tristani-Firouzi, M., 2017. CRISPR/Cas9-Directed Gene Editing for the Generation of Loss-of-Function Mutants in High-Throughput Zebrafish F_0 Screens, in: Current Protocols in Molecular Biology. John Wiley & Sons, Inc., Hoboken, NJ, USA, pp. 31.9.1-31.9.22. https://doi.org/10.1002/cpmb.42

Singh, C., Rihel, J., and Prober, D.A., 2017. Neuropeptide Y Regulates Sleep by Modulating Noradrenergic Signaling. Curr. Biol. 27, 3796-3811.e5. https://doi.org/10.1016/J.CUB.2017.11.018

Sivasubbu, S., Balciunas, D., Amsterdam, A., and Ekker, S.C., 2007. Insertional mutagenesis strategies in zebrafish. Genome Biol. https://doi.org/10.1186/gb-2007-8-s1-s9

Stavropoulos, N., and Young, M.W., 2011. insomniac and Cullin-3 regulate sleep and wakefulness in Drosophila. Neuron 72, 964–76. https://doi.org/10.1016/j.neuron.2011.12.003

Sugimoto, H., Ikeda, K., and Kawakami, K., 2014. Heterozygous mice deficient in Atp1a3 exhibit motor deficits by chronic restraint stress. Behav. Brain Res. 272, 100–110. https://doi.org/10.1016/j.bbr.2014.06.048

Sweadner, K.J., and Rael, E., 2000. The FXYD gene family of small ion transport regulators or channels: cDNA sequence, protein signature sequence, and expression. Genomics

68, 41–56. https://doi.org/10.1006/geno.2000.6274

Thisse, C., and Thisse, B., 2008. High-resolution in situ hybridization to whole-mount zebrafish embryos. Nat. Protoc. 3, 59–69. https://doi.org/10.1038/nprot.2007.514

Toda, H., Williams, J.A., Gulledge, M., and Sehgal, A., 2019. A sleep-inducing gene, nemuri, links sleep and immune function in Drosophila. Science 363, 509–515. https://doi.org/10.1126/science.aat1650

Ulitsky, I., Shkumatava, A., Jan, C.H., Sive, H., and Bartel, D.P., 2011. Conserved function of lincRNAs in vertebrate embryonic development despite rapid sequence evolution. Cell 147, 1537–1550. https://doi.org/10.1016/j.cell.2011.11.055

Varshney, G.K., Lu, J., Gildea, D.E., Huang, H., Pei, W., Yang, Z., Huang, S.C., Schoenfeld, D., Pho, N.H., Casero, D., et al., 2013. A large-scale zebrafish gene knockout resource for the genome-wide study of gene function. Genome Res. 23, 727–35. https://doi.org/10.1101/gr.151464.112

Villalba, A., Coll, O., and Gebauer, F., 2011. Cytoplasmic polyadenylation and translational control. Curr. Opin. Genet. Dev. 21, 452–457. https://doi.org/10.1016/j.gde.2011.04.006

Wilkinson, R.N., Elworthy, S., Ingham, P.W., and van Eeden, F.J.M., 2013. A method for high-throughput PCR-based genotyping of larval zebrafish tail biopsies. Biotechniques 55, 314–316. https://doi.org/10.2144/000114116

Wu, M., Robinson, J.E., and Joiner, W.J., 2014. SLEEPLESS Is a Bifunctional Regulator of Excitability and Cholinergic Synaptic Transmission. Curr. Biol. 24, 621–629. https://doi.org/10.1016/j.cub.2014.02.026

Wu, M.N., Koh, K., Yue, Z., Joiner, W.J., and Sehgal, A., 2008. A Genetic Screen for Sleep and Circadian Mutants Reveals Mechanisms Underlying Regulation of Sleep in Drosophila. Sleep 31, 465–472. https://doi.org/10.1093/sleep/31.4.465

734 Wu, R.S., Lam, I.I., Clay, H., Duong, D.N., Deo, R.C., and Coughlin, S.R., 2018. A Rapid
735 Method for Directed Gene Knockout for Screening in G0 Zebrafish. Dev. Cell 46, 112-
736 125.e4. https://doi.org/10.1016/j.devcel.2018.06.003

737 Yokogawa, T., Marin, W., Faraco, J., Pézeron, G., Appelbaum, L., Zhang, J., Rosa, F.,
738 Mourrain, P., and Mignot, E., 2007. Characterization of sleep in zebrafish and insomnia
739 in hypocretin receptor mutants. PLoS Biol. 5, e277.
740 https://doi.org/10.1371/journal.pbio.0050277

741 Zhang, Y., Chen, K., Sloan, S.A., Bennett, M.L., Scholze, A.R., O'Keeffe, S., Phatnani, H.P.,
742 Guarnieri, P., Caneda, C., Ruderisch, N., et al., 2014. An RNA-sequencing transcriptome
743 and splicing database of glia, neurons, and vascular cells of the cerebral cortex. J.
744 Neurosci. 34, 11929–11947. https://doi.org/10.1523/JNEUROSCI.1860-14.2014

745

746

MATERIALS AND METHODS

Zebrafish husbandry

All zebrafish lines were housed on a 14hr:10hr light:dark schedule in dechlorinated water at 27.5^{o}C and routine husbandry was performed by the UCL Zebrafish Facility. Embryos were collected from spontaneous spawning and staged according to Kimmel et al. 1995.

Embryos and larvae were raised on a 14hr:10hr light:dark schedule in 10cm Petri dishes at a density of 50 embryos per 10cm Petri dish. Embryo water (~pH7.3, temperature 28.5^{o}C, conductivity ~423.7uS with methylene blue) was changed daily and animals over 4 days post fertilisation were euthanized by overdose of MS-222 (300 mg/l) or 15% 2-Phenoyethanol (77699 SIGMA-ALDRICH) at the end of experiments.

Raising of genetically altered zebrafish and all experimental procedures were performed under project licence 70/7612 and PA8D4D0E5 awarded to JR under the UK Animals (Scientific Procedures) Act 1986 guidelines.

Lines

Strain designation	**Gene identifier**	**Additional Information**
10543/dmist^{vir}	ENSDARG00000095754	Line maintained at J Rihel lab
dmist^{i8}	ENSDARG00000095754	Line maintained at J Rihel lab
fxyd1$^{\Delta 28}$	ENSDARG00000099014	Line maintained at J Rihel lab
atp1a3a$^{\Delta 19}$	ENSDARG00000018259	Line maintained at J Rihel lab
atp1a3b $^{\Delta 14}$	ENSDARG00000104139	Line maintained at J Rihel lab

Table 1. Zebrafish lines

763 The *dmist*^{vir} allele was generated in wild type line T/AB-5 (Varshney et al., 2013) and
764 outcrossed to Harvard AB. The *dmist*^{i8}, *fxyd1* $^{\Delta 28}$, *atp1a3a*$^{\Delta 19}$, and *atp1a3b* $^{\Delta 14}$ alleles were
765 generated and maintained at UCL on an AB/TL background. Both *dmist*^{i8} and *dmist*^{vir} were out-
766 crossed to the AB strain at UCL for 3 generations.

767 *Larval Tracking*

768 At 4 days post fertilisation (dpf), zebrafish larvae were placed into individual wells of a 96-
769 square well plate (WHA7701-1651 Sigma-Aldrich) filled with 650 µl of embryo water per well
770 and tracked for 3 days under a 14:10 light:dark schedule (lights on-09:00, lights off-23:00) using
771 automated videotracking in ViewPoint ZebraBoxes (Viewpoint Life Sciences). The 96-well plate
772 was under constant illumination with infrared LEDs, and white LEDs simulated the light:dark
773 schedule. Videography (with one-third inch Dragonfly2 PointGrey monochrome camera, frame
774 rate: 25-30 Hz; fixed-angle megapixel lens, Computar M5018-MP) of individual larval activity
775 was recorded in quantization mode to detect movement by background subtraction between
776 frames in individual wells with 60 second integration time bins. Parameters used for detection
777 were calibrated according to the sensitivity of individual boxes but were in the following range:
778 detection threshold, 15-20; burst, 50 pixels; freeze, 3-4 pixels. Embryo water in the wells was
779 topped up daily with fresh water, and ambient room temperature was maintained at
780 approximately 26^{o}C. Output data was sorted, parsed and analysed by custom Perl and Matlab
781 scripts (MATLAB R2016 version 9.1, The MathWorks), as in Rihel et al. 2010.

782 Oxygen-permeable lids (Applied Biosystems 4311971) were applied over the top of the 96-
783 well plate when performing experiments in constant darkness, and the larvae were left
784 undisturbed for the duration of the experiment to avoid light exposure.

785 At the end of the experiment, all larvae were visually checked for health before euthanasia
786 and transfer to individual wells of a 96-well PCR plate for DNA extraction and genotyping.

Behavioural analysis

Sleep parameters were calculated as in Rihel et al. 2010. Behavioural summaries across multiple experiments were determined by using the Matlab fitlme function to fit a linear mixed effects model for each parameter with genotype as a fixed effect and independent experiment as a random effect, then representing the effect size as a % change from the wild type value. Before fitting the linear mixed effects model, the parameters sleep, sleep length, and waking activity were log normalized by calculating the log of 1+ the parameter value for each larva.

Circadian period for every larvae was calculated using the Matlab findpeaks function on the activity (delta-pixels) timeseries data with a minimum peak distance of 18 hours (1080 minutes). N-way ANOVA was calculated to evaluate differences between groups.

Code and data are available at https://github.com/ilbarlow/Dmist.

Adult tracking

Fish from a *dmist*$^{i8/+}$ x *dmist*$^{i8/+}$ cross were raised in a mixed gender tank to adulthood. Zebrafish adults (aged 3-4 months) were randomly selected and tracked on a 14:10 light:dark cycle (180 lux at water surface, lit from above) for three days as in (Chiu et al., 2016). In brief, fish were placed into uncovered plastic chambers (7x12x8.5 cm; WxLxH) with small holes for water exchange, and these were placed in a circulating water tank (46x54 cm with 4.5 cm water height). This setup was supplied with fish water from the home aquarium heated to 28ºC and pumped from a 45L reservoir at a flow rate of 1.3 L/min. Infrared light (60 Degree, 54 LED Video Camera Red Infrared Illuminator Lamp, SourcingMap, with the ambient light detector covered) was continuously supplied from below. Fish were tracked at 15 Hz using Viewpoint Life Sciences ZebraBox tracking software in tracking mode, with a background threshold of 40, inactive cut-off of 1.3 cm/sec, and a small movement cut-off of 8 cm/sec. Each track was visually inspected for errors at one-minute resolution across the entire session and analysed using custom Matlab scripts (MATLAB R2016 version 9.1, The Mathworks, Inc). During the

812 tracking, the experimenter was blinded to genotype, which was determined by fin-clip after the
813 experiment. Females and males were originally analysed separately; since no significant
814 gender effect was found (two-way ANOVA, genotypeXgender), data from both genders were
815 pooled for the final analysis.

816 *Genotyping*

817 Prior to genotyping, adult fish were anaesthetised in 30 µg/ml MS-222, fin-clipped by cutting
818 a small section of the caudal fin, and then allowed to recover in fresh fish water. For pooled
819 experiments, 3dpf larvae from heterozygous in-crosses were fin-clipped as in Wilkinson et al.,
820 2013 and allowed to recover in a square 96-well plate to keep larvae separate prior to pooling
821 larvae of the same genotype. Genomic DNA was extracted from adult fin clips and larvae by
822 boiling for 30 minutes in 50 µl 1X base solution (0.025 M KOH, 0.2 mM EDTA). Once cooled,
823 an equal volume (50 µl) of neutralisation buffer (0.04 M Tris-HCl) was then added and undiluted
824 genomic DNA used for genotyping.

825 The *dmist*^{vir} genotype was detected by PCR (standard conditions) using a cocktail of three
826 primers (0.36 mM final concentration each primer) to detect the wild type allele and viral
827 insertion (see Table 2) so that genotypes could be assigned according to size of bands
828 detected (*dmist*$^{vir/vir}$ 800bp; *dmist*$^{vir/+}$ 508bp and 800bp; *dmist*$^{+/+}$ 508bp).

829 The *dmist*^{i8} genotype was assigned by KASP genotyping using allele-specific primers
830 (*dmist*^{i8} allele 5'-GATCTCCCT[GCAGAAAGAT]CTTTCTGCA-3' = FAM, *dmist*$^{+}$ allele 5'-
831 GATCTCCCT[CACCG]CTTTCTGCA-3' = HEX; KASP mastermix KBS-1016-011) and assay
832 were prepared and analysed according to manufacturer's protocol (LGC genomics).

833 The *atp1a3a*$^{\Delta 19}$ genotype was assigned by KASP genotyping using allele-specific primers
834 (*atp1a3a*$^{\Delta 19}$ allele 5'-

GACAGACTGAAGAAACAGCGACTGACGGCTC[CAAAATGGGGGTAAGAGTC]-3' = FAM, *atp1a3a*$^{+}$ allele 5'-GACAGACTGAAGAAACAGCGACTGACGGCTC-3'[] = HEX).

The *atp1a3b* $^{\Delta 14}$ genotype was assigned by PCR using MiSeq_atp1a3b primers (Table 2), with the *atp1a3b* $^{\Delta 14}$ allele running 14bp faster then the *atp1a3b*$^{+}$ allele.

fxyd1$^{\Delta 28}$ was assigned by KASP genotyping using allele-specific primers (*fxyd1*$^{\Delta 28}$ allele 5'-GAAGGTCGGAGTCAACGGATTTAATAAACTTTATTGTGCTTTTGTAGTTGT[A]-3' = HEX, *fxyd1*$^{+}$ allele 5'-GAAGGTGACCAAGTTCATGCTTAATAAACTTTATTGTGCTTTTGTAGTTGT[G]-3' = FAM) or PCR using MiSeq_fxyd1 primers (see Table 2) followed by digestion with the restriction enzyme DrdI, which yields bands at 138bp and 133bp for *fxyd1*$^{+/+}$; 138bp, 133bp and 271bp for *fxyd1*$^{+/\Delta 28}$, and 243bp for *fxyd1*$^{\Delta 28}$.

3'RACE

FirstChoice RLM-RACE kit (Ambion AM1700) was used to amplify the 5' and 3' ends from cDNA obtained from 4dpf larvae raised on a 14:10 LD cycle and C57BL/6 E13.5 mouse embryos obtained from Parnavalas lab (UCL). 5' and 3'RACE primers were designed according the manufacturer's guidelines (Table 2) and the manufacturer's protocol was followed. Clones were sequenced by Sanger sequencing.

In situ hybridisation

Probes were designed to target the 3'UTR and entire open reading frame (ORF) of *dmist_Dr* transcript using primers that amplified the target region from zebrafish cDNA under standard PCR conditions (expected size 1325bp; Table 2). The PCR product was cloned into pSC vector (Strataclone PCR cloning kit Agilent 240205-12) and verified by Sanger sequencing. Antisense probe was generated by cleavage of pSC-dmist plasmid with XbaI and *in vitro* transcribed with T3 polymerase (Promega P2083) using 1 μg DNA template according to standard *in vitro*

transcription protocol (see full protocol at dx.doi.org/10.17504/protocols.io.ba4pigvn). RNA probe was extracted and purified using ZYMO RNA concentrator kit (Zymo #R1013).

Whole mount *in situ* hybridisation was performed according to (Thisse and Thisse, 2008) with the following adaptations. Embryos <5dpf were dechorionated and fixed at the appropriate stage in 4% paraformaldehyde (PFA) overnight at 4ºC. 5dpf larvae were fixed in 4% PFA/4% sucrose overnight at 4ºC and then washed 3x5mins in PBS prior to dissecting out the brain. Fixed embryos were washed 3x5mins in PBS, progressively dehydrated into 100% methanol (MeOH) and stored at -20ºC overnight. Prior to pre-hybridisation embryos were bleached for 30 mins in the dark (0.05% formamide, 0.5X SSC, 6% H_2O_2) and then fixed in 4% PFA for 30 mins at room temperature. To image, the embryos were progressively rehydrated into 0.1% PBTw, progressively sunk in to 80% glycerol, and imaged on Nikon compound microscope (Nikon Eclipse Ni, Leica MC190HD camera).

RT-qPCR

Larvae from heterozygous in-crosses (*dmist*$^{i8/+}$ or *dmist*$^{vir/+}$) were genotyped at 3dpf and allowed to recover fully before euthanizing at 5dpf. RNA was extracted from three 5dpf embryos of each genotype by snap freezing in liquid nitrogen and TRIzol RNA extraction (Ambion 15596026) with the following modifications to the manufacturer's protocol: 400 µl total TRIzol reagent used to homogenise larvae using a pellet pestle homogenizer, and 5 µg glycogen (Invitrogen Cat No. 10814010; 20 µg/µl) was added to the RNA solution after chloroform extraction to aid precipitation of the RNA. The cDNA library was synthesised from high quality RNA (Agilent AffinityScript qPCR cDNA synthesis kit 600559), diluted 1:10, and gene-specific primers (Table 2) were used for amplification of target genes with SYBR green mastermix in BioRad CFX Real-Time qPCR instrument. The expression levels were normalised to the housekeeping gene *EF1alpha* (primers in Table 2) and analysed using custom Matlab scripts (MATLAB v9.2 2017, The Mathworks 2017).

Sodium Green Assay

Cell permanent Sodium Green tetraacetate (Invitrogen, S6901) was prepared fresh from frozen stock by dissolving in DMSO to 1 mM then diluting in fish water to a final concentration of 10 µM. About 50 larvae (5-7 dpf) from *atp1a3a*$^{\Delta 19/+}$ or dmist$^{i8/+}$ in-crosses were placed in wells of a 6 well plate, then most fish water was removed and replaced with 3 mL of the 10 µM Sodium Green solution for two hours. During exposure, the plate was covered in foil and placed in a 28°C incubator. For PTZ experiments, larvae were also exposed to 10 mM PTZ (diluted from 1mM stock dissolved in water) for two hours. For timepoints at night (ZT17-19), larvae were handled and collected under red light. After soaking in Sodium Green, larvae were washed 3X with fish water, anaesthetised with MS-2222, and fixed in 4% PFA/4% sucrose overnight at 4°C. After 3X wash in PBS, larval brains were dissected and placed in 200 µL PBS in a 48 well plate, and the matched bodies were used for genotyping (see Genotyping). Brains were imaged using an upright MVX10 MacroView microscope with an MC PLAPO 1x objective (both OLYMPUS) with a mercury lamp for fluorescent excitation at 488 nm (OLYMPUS, U-HGLGPS). Images of roughly the same focal plane (dorsal/ventral view) were taken with an XM10 OLYMPUS camera by a single exposure following minimal light exposure (to avoid bleaching). Mean fluorescent intensity was calculated from ROIs placed on the optic tectum/midbrain using ImageJ and normalized to the average fluorescence intensity for each imaging session.

Protein Alignments

Cross-species *dmist* homologues were identified by reciprocal BLASTp of C-terminal region of Dmist_*Dr* in vertebrate genomes. Translations of candidate transcript open reading frames were then aligned with Dmist_*Dr* using ClustalOmega to calculate the percentage identity matrix (www.ebi.ac.uk/Tools/msa/clustalo/) and visualised with the tool Multiple Align Show (www.bioinformatics.org/sms/multi_align.html).

To identify Dmist orthologues, Dmist peptides were aligned with the multiple sequence alignment tool MAFFT (Katoh and Toh, 2010) and seeded into a JackHMMR iterative search of the Uniprot database (Johnson et al., 2010). Protein-protein alignments of Dmist to Fxyd1 were then performed using ClustalOmega and visualized with the tool Multiple Align Show.

CRISPR/Cas9 gene targeting

CRISPR targets were designed and synthesised according to Gagnon et al., 2014 using ChopChop (Montague et al. 2014; http://chopchop.cbu.uib.no/; see Table 2 for sequences) to identify target sites. 100 pg sgRNA and 300 pg Cas9 mRNA (pT3TS-nCas9n) were injected into the yolk of 1-cell stage AB-TL embryos obtained from natural spawning. F0 fish were screened by high resolution melt (HRM) analysis using gene-specific primers (Table 2) with Precision melt supermix (Biorad 1725112) according to the manufacturer's protocol in a BioRad CFX RT-PCR thermocycler. Positive founders identified in HRM analysis were then sequenced by Illumina MiSeq sequencing using gene specific primers with adapters (Table 2) according to the manufacturer's protocol.

Molecular cloning

GFP was fused to the Dmist_*Dr* open reading frame (ORF) by Gateway cloning (Kwan et al., 2007). Gene-specific primers were designed to amplify a PCR product that was recombined with middle donor vector (Table 2; Invitrogen Gateway pDONR221 Cat No. 12536017, Invitrogen Gateway BP Clonase II Cat No. 11789020) to generate a middle entry clone (pME-Dmist). pME-Dmist was recombined with 5' (p5E-CMV/SP6) and 3' (p3E-GFPpA) entry clones and destination vector (pDestTol2pA2) using Gateway Technology (Invitrogen LR Clonase II Plus enzyme Cat No. 12538200) following the manufacturer's protocol.

A 3bp mutation was introduced into the *CMV:dreammist-GFPpA* by inverse PCR using specific primers (Table 2) and KOD high fidelity hot start polymerase (Millipore 71085). The template was degraded by DpnI digest and circular PCR product was transformed into

933 OneShot TOP10 chemically competent E coli (Invitrogen C4040). Both *CMV:dreammist-*
934 *GFPpA* and *CMV:dreammistA22W-GFPpA* constructs were checked by Sanger sequencing.

935 For labelling the plasma membrane, mRNA was *in vitro* transcribed from pCS2-myr-Cherry
936 linearlised with Not1, *in vitro* transcribed with SP6 mMessage mMachine (Ambion AM1340),
937 purified and quantified with a QuBit spectrophotometer, and injected at 0.04 μg/μL.

938 *Microinjection and imaging*

939 For Dmist-GFP and DmistA22W-GFP live imaging, embryos from an AB-TL in-cross were
940 injected with 1 nL of plasmid (7 ng/μL). After developing to 90% epiboly, the embryos were
941 placed on a glass coverslip and observed on an inverted confocal microscope (SPinv, Leica)
942 with a 40X objective.

943 *RNAseq*

944 Larvae from heterozygous in-crosses (*dmist*$^{i8/+}$ x *dmist*$^{i8/+}$ and *dmist*$^{vir/+}$ x *dmist*$^{vir/+}$) were
945 raised to adulthood, genotyped and then homozygous and wild type siblings kept separate.
946 Homozygous and wild-type sibling fish were then in-crossed so that first cousins were directly
947 compared. RNA was extracted from 30 6dpf larvae using the same protocol as for RT-qPCR
948 and sent for RNAseq analysis at the UCL Institute of Child Health with a sequencing depth of
949 75 million reads per sample. Differential analysis of transcript count level between groups was
950 performed as in Love et al., 2014 and additional analysis was performed using custom Matlab
951 scripts (MATLAB v9.2 2017, The Mathworks 2017).

952 *Mouse RNAseq analysis*

953 The dataset was downloaded from
954 (https://web.stanford.edu/group/barres_lab/brain_rnaseq.html; Zhang et al., 2014) and
955 hierarchical clustering (average linkage) and Pearson correlation calculation analysis were
956 performed using custom Matlab scripts (MATLAB v9.2 2017, The Mathworks 2017).

957 *Experimental Design and Statistical Analyses*

958 Data was tested for normality using the Kolmogorov-Smirnov test. If data were normally
959 distributed, N-way ANOVA (alpha=0.05) was used with correction for multiple comparisons
960 using Tukey's test. If non-parametric, the Kruskal-Wallis test was used with correction for
961 multiple comparisons using Dunn-Sidak (alpha=0.05). Outliers were removed by Grubb's test
962 (threshold $p<0.01$). Data were grouped by genotype and gender for adult experiments and
963 grouped by genotype and day of experiment for larval experiments.

964 All code is available at https://github.com/ilbarlow/Dmist.

965 **Table 2. Primer Sequences**

966

	Oligo Name	Sequence (5' -> 3')	Annealing temperature (oC)	Application
1	dmist_vir_fw	CACAGGGATGTGATGCCGGTTAAC	55	dmistvir genotyping
2	dmist_vir_rev	GTAGACACATACTGCCATACCAATC	55	dmistvir genotyping
3	vir_fw	CACCAGCTGAAGCCTATAGAGTACGAGC-	55	dmistvir genotyping
4	dmist_Dr_5RACE_fw	CGTTTCGCCACAATGTCAGCA	55-65	dmist_Dr 5'RACE
5	dmist_Dr_5RACE_rev_outer	AATGTTCAACTCCAGGCGTC	55-65	dmist_Dr 5'RACE
6	dmist_Dr_5RACE_rev_inner	AATGTTCAACTCCAGGCGTC	55-65	dmist_Dr 5'RACE
7	dmist_Dr_3RACE_fw_inner	GACGCCTGGAGTTGAACATT	55-65	dmist_Dr 3'RACE
8	dmist_Dr_3RACE_fw_outer	GGTATGGCAGTATGTGTCTACA	55-65	dmist_Dr 3'RACE
9	Dmist_Mm_3RACE_outer	GCTGGTGACTGTCCTCCTTATG	55-65	dmist_Mm 3'RACE
10	Dmist_Mm_3RACE_inner	GTGTCTACAAGCCCATCCGTC	55-65	dmist_Mm 3'RACE
11	dmist_Dr_fw	TTTCGCCACAATGTCAGCAGC	56	dmist_Dr probe
12	dmist_Dr_rev	CGACTTTCATTTATTAGTTCAGACATGTC	56	dmist_Dr probe
13	qPCR_dmist_fw	ACGCCAGACCTTATGAAATCC	60	RT-qPCR
14	qPCR_dmist_rev	TGCGTCGGAGAGGTTTGTAG	60	RT-qPCR
15	qPCR_ankrd13a_fw	TGGTGGCGTTCCAGAGTTAC	60	RT-qPCR
16	qPCR_ankrd13a_rev	GGACACGAGAGGAATCCAGC	60	RT-qPCR
17	qPCR_slc6a4b_fw	ACATGGTTGGGTCGACGTTT	60	RT-qPCR
18	qPCR_slc6a4b_rev	TCCAACCCACCAAAAGTGCT	60	RT-qPCR
19	ef1alpha_fw	TGCTGTGCGTGACATGAGGCAG	60	RT-qPCR
20	ef1alpha_rev	CCGCAACCTTTGGAACGGTGT	60	RT-qPCR
21	SP6dmist_sgRNA	ATTTAGGTGACACTATAGCGTTATGCAGAAAGCGGTGGTTTTAGAGCTAGAAATAGCAAG	n/a	CRISPR
22	T7atp1a3a_sgRNA	TAATACGACTCACTATAGACTGACGGCTCCAAAATGGGTTTTAGAGCTAGAAATAGCAAG	n/a	CRISPR
23	SP6fxyd1_sgRNA	ATTTAGGTGACACTATAGGACCCTCTGCCAACACAAGGTTTTAGAGCTAGAAATAGCAAG	n/a	CRISPR
24	SP6atp1a3b_sgRNA	ATTTAGGTGACACTATAGGACTGACTGCGCAACCATGGTTTTAGAGCTAGAAATAGCAAG	n/a	CRISPR
25	HRM_dmist_fw	GCCACAATGTCAGCAGCACG	59	HRM
26	HRM_dmist_rev	GCGTTCACTTTAGACTCTCCCAGC	59	HRM
27	HRM_atp1a3a_fw	TGACAGACTGAAGAAACAGC	55	HRM
28	HRM_atp1a3a_rev	TTAAATCTCAGCACCAGCAG5	55	HRM
29	HRM_fxyd1_fw	TGACCAAACCTTCTTAAGGTGC	58	HRM
30	HRM_fxyd1_rev	AAATTGAGAAGACTTACTGGTCTGC	58	HRM
31	HRM_atp1a3b_fw	AAAGGCTGTCACTTTCTCCATCAC5	58	HRM
32	HRM_atp1a3b_rev	TGCAGTAGATGAGGAATCGGTC	58	HRM
33	MiSeq_dmist_fw	TCGTCGGCAGCGTCAGATGTGTATAAGAGACAGTATAACTTACGTGTGGACGGACTC	58	MiSeq
34	MiSeq_dmist_rev	GTCTCGTGGGCTCGGAGATGTGTATAAGAGACAGTTGCCTCAGCAGGATTTCATAAG	58	MiSeq
35	MiSeq_atp1a3a_fw	TCGTCGGCAGCGTCAGATGTGTATAAGAGACAGTCGTTATCCGTGCAAGAGCTTC	58	MiSeq
36	MiSeq_atp1a3a_rev	GTCTCGTGGGCTCGGAGATGTGTATAAGAGACAGTTCTCAGCACCAGCAGTTATCG	58	MiSeq
37	MiSeq_atp1a3b_fw	TCGTCGGCAGCGTCAGATGTGTATAAGAGACAGTGACTGACATTCTCTCTTCGTG	68	MiSeq
38	MiSeq_atp1a3b_rev	GTCTCGTGGGCTCGGAGATGTGTATAAGAGACAGTTCTCTGTGATGCAGTAGATGAGG	68	MiSeq
39	MiSeq_fxyd1_fw	TCGTCGGCAGCGTCAGATGTGTATAAGAGACAGAAATACTGTCTTGTGACCAAACC	57	MiSeq
40	MiSeq_fxyd1_rev	GTCTCGTGGGCTCGGAGATGTGTATAAGAGACAGTTCATCCTCTGCTGCAAAATGC	57	MiSeq
41	attB1-dreammist forward primer	GGGGACAAGTTTGTACAAAAAAGCAGGCTTCACCATGTCAGCAGCACGCCTGATCTCC	55-60	Gateway
42	attB3-dreammist reverse primer	GGGGACCACTTTGTACAAGAAAGCTGGGTATCACCTGCGTCGGAGAGGTTTGTAG	55-60	Gateway
43	Dmist-GFPA22WFw	GCTTTTCCAGTCTGGGAGT**TGG**CAGCTGGGAGAGTCTAAAG	66	SDM
44	Dmist-GFPA22WRev	CTTTAGACTCTCCCAGCTG**CCA**ACTCCCAGACTGGAAAAGC	66	SDM

967 # FIGURE LEGENDS

968

969 **Figure 1. A viral insertion mini-screen identifies a short-sleeping mutant, *dreammist.***

970 A-B) Representative 48hr mean sleep (A) and waking activity (B) traces of progeny from
971 *dmist*$^{vir/+}$ in-cross from the initial screened clutch. White blocks show day (lights on) and
972 grey blocks show night (lights off). The ribbon around each trace indicates standard error
973 of the mean.

974 C-F) Analysis of sleep/wake architecture of *dmist*$^{vir/vir}$ in the original screen during the day
975 (white panel) and night (grey panel). C) Quantification of total sleep across two days and
976 nights shows decreased day and night sleep in *dmist*$^{vir/vir}$. Analysis of sleep architecture
977 reveals fewer sleep bouts during the day (D) and shorter sleep bouts at night (E) in *dmist*$^{vir/vir}$
978 compared with sibling controls. F) Daytime waking activity is also increased in *dmist*$^{vir/vir}$.
979 (*dmist*$^{+/+}$ n=38, *dmist*$^{vir/+}$ n=84, *dmist*$^{vir/vir}$ n=19). The black lines show the mean ± SEM,
980 except in E, which labels the median. *p<0.05, **p<0.01, ***p<0.001; one-way ANOVA,
981 Tukey's post hoc test.

982 G) Combining N=5 independent tracking experiments using a linear mixed effects model
983 with genotype as a fixed effect and experiment as a random effect reveals *dmist*$^{vir/vir}$ larvae
984 have decreased total sleep and changes to sleep architecture during both the day and night
985 compared to *dmist*$^{+/+}$ siblings. Plotted are the genotype effect sizes (95% confidence
986 interval) on each parameter relative to wild type. Shading indicates day (white) and night
987 (grey), and p-values are assigned by an F-test on the fixed effects coefficients from the
988 linear mixed effects model. *p<0.05, **p<0.01, ***p<0.001, ns p>0.05

989

Figure 2. *dmist* encodes a conserved vertebrate single pass transmembrane protein.

A) *dmist* mutants harbour a viral insertion in the 1st intron of *si:key0234h16.7*. *dmist* is syntenic with *ankrd13* and *GIT* in mouse, human, and zebrafish.

B) Quantitative RT-qPCR of *dmist* (red) show reduced expression of *dmist* and not the 5' and 3' flanking zebrafish genes, *slc6a4b* (cyan) and *ankrd13a* (blue), in *dmist*$^{vir/vir}$ larvae compared to *dmist*$^{vir/+}$ and *dmist*$^{+/+}$ siblings. **p<0.01, *p<0.05; one-way ANOVA, Tukey's post-hoc test. Data shows mean ± SEM normalized to the wild type mean.

C) *dmist_Dr* contains an open reading frame encoding a 70 amino acid protein that is conserved across vertebrates. All identified homologues have a predicted signal peptide sequence (magenta line), signal peptide cleavage site (magenta circle), and predicted transmembrane domain (grey), with additional highly conserved C-terminal small peptide motifs (blue lines). Identical amino acids in all species are shown in black; similar amino acids (80-99% conserved across species) are shown in grey.

D) *In situ* hybridisation using *dmist* antisense probe reveals *dmist* is maternally deposited as it is detected at the 2-cell stage. At 24hpf expression is restricted to regions containing neuronal precursors, and at 5dpf expression is widespread throughout the brain. Tel, telencephalon; Dien, diencephalon; R1-6, rhombomeres 1-6. Scale bars= 0.5 mm (2 cell and 24 hpf), 0.1 mm (5 dpf).

E-F) Representative confocal image of 90% epiboly embryo co-injected at the 1-cell stage with mRNA encoding either C-terminal tagged Dmist-GFP (E, green) or DmistA22W-GFP (F, green) and membrane-RFP (magenta). Scale bar= 25 μm.

Figure 3. CRISPR-generated *dmist* mutants sleep less and are hyperactive at night.

A) CRISPR/Cas9 targeting of the first exon in *dmist* resulted in an 8bp insertion (*dmist*^{i8}) (grey line) within the coding sequence leading to an early stop codon (red line with *).

B) Predicted Dmist^{i8} peptide sequence lacks most of the N-terminal signal peptide sequence (magenta) and the full C-terminus.

C-D) Representative 48 hr traces of sleep (C) and waking activity (D) for *dmist*$^{i8/i8}$ fish compared to *dmist*$^{i8/+}$and *dmist*$^{+/+}$ siblings shows decreased sleep and increased waking activity at night. Mean ±SEM is shown. n=number of animals.

E-H) Analysis of sleep/wake architecture of the experiment depicted in (C, D) indicates that *dmist*$^{i8/i8}$ larvae sleep less at night (E) due to fewer sleep bouts (F). Sleep bout length is unchanged (G). Waking activity was also increased in *dmist*$^{i8/i8}$ fish (H). The black line represents the mean ± SEM except for G, which is the median. *p<0.05, **p<0.01, ***p<0.001; One-way ANOVA, Tukey's post hoc test.

I) Combining 5 independent experiments with a linear mixed effects model reveals *dmist*$^{i8/i8}$ fish sleep less due to fewer sleep bouts, and also show increased waking activity at night. Plotted are the genotype effect sizes (95% confidence interval) on each parameter relative to wild type. Shading indicates day (white) and night (grey). P-values are assigned by an F-test on the fixed effects coefficients from the linear mixed effects model. *p<0.05, **p<0.01, ***p<0.001, ns p>0.05

J) *dmist*$^{i8/i8}$ larvae have increased rebound sleep compared to wild type siblings following exposure to 5mM PTZ. Representative sleep traces of *dmist*$^{+/+}$ (no drug, water vehicle controls in black; PTZ exposed in blue) and *dmist*$^{i8/i8}$ (no drug in purple; PTZ exposed in red) following 1 hr exposure to 5mM PTZ (black bar) in the morning. Data are mean ±SEM. *dmist*$^{i8/+}$ animals are not plotted for clarity but are included in panel K.

K) Rebound sleep after exposure to 5mM PTZ, calculated from the experiment in J. Each dot represents a single larva, grey lines show mean ± SEM. As shown in Figure S4C, normalizing the PTZ responses to the mean control baselines for each genotype shows that *dmist*$^{i8/i8}$ fish have a significantly increased response relative to their sibling controls. ($p<0.05$, one-way ANOVA).

L-M) Adult *dmist*$^{i8/i8}$ fish are more active at night. 48-hour centroid tracking shows *dmist*$^{i8/i8}$ adults have a higher mean swim speed compared to their wild type siblings (L). Mean speed at night is quantified in M (cross shows mean ± SEM). *$p<0.05$, one-way ANOVA.

Figure 4. Mutation of the *dmist* related gene *fxyd1* causes reduced sleep at night.

A) Schematic of zebrafish Dmist and Fxyd1 protein domains and alignments comparing human, mouse, and zebrafish Dmist and FXYD1 protein sequences. Black and grey shading indicate amino acid identity and similarity, respectively. The FXYD domain is highlighted with a red line and the RRR motif in the C-terminus is indicated with a blue line.

B) CRISPR-Cas9 targeting of the 3rd exon of *fxyd1* created a 28 bp deletion predicted to encode a truncated protein. The start codon is marked by a blue line. Guide RNA target sequence and PAM sequence are shown as grey bars.

C) *In situ* hybridisation of *fxyd1* at 24hpf (whole animal) and 5dpf brain (ventral view). Anterior is to the left. Scale bar = 0.5 mm (24hpf); 0.1 mm (5 dpf).

D-E) Representative single tracking experiment showing *fxyd1*$^{\Delta 28}$ mutants have decreased night-time sleep (D) but normal waking activity (E).

F) Combining 5 independent experiments with a linear mixed effects model reveals *fxyd1*$^{\Delta 28/\Delta 28}$ larvae sleep significantly less at night due to a shorter sleep bout length compared to *fxyd1*$^{+/+}$ siblings. Plotted are the genotype effect sizes (95% confidence interval) on each parameter relative to wild type. Shading indicates day (white) and night (grey). P-values are assigned by an F-test on the fixed effects coefficients from the linear mixed effects model. *p<0.05, **p<0.01, ***p<0.001, ns p>0.05

Figure 5. Mutations in the Na+/K+ pump alpha subunit *atp1a3a* reduces sleep at night

A) CRISPR-Cas9 targeting of the *atp1a3a* resulted in a 19 bp deletion that eliminates the start codon (blue) and splice junction.

B) CRISPR-Cas9 targeting of *atp1a3b* resulted in a 14 bp deletion that eliminates the start codon (blue)..

C) *In situ* hybridisation of *atp1a3a* and *atp1a3b* at 24hpf (whole animal) and 5dpf brain (ventral view). Anterior is to the left. Scale bar = 0.5 mm (24 hpf); 0.1 mm (5 dpf).

D) Representative single tracking experiment showing *atp1a3a*$^{\Delta 19/\Delta 19}$ fish are hyperactive throughout the day-night cycle and have decreased sleep at night.

E) Representative single tracking experiment showing *atp1a3b*$^{\Delta 14/\Delta 14}$ mutants have increased daytime waking activity but normal sleep patterns.

F) *atp1a3a*$^{\Delta 19/\Delta 19}$ larvae sleep less at night due to shorter sleep bouts. Plotted are the genotype effect sizes (95% confidence interval) on each parameter relative to wild type. Shading indicates day (white) and night (grey). P-values are assigned by an F-test on the fixed effects coefficients from the linear mixed effects model. *p<0.05, **p<0.01, ***p<0.001, ns p>0.05

G) Brain sodium levels are significantly elevated after exposure to PTZ in both *atp1a3a*$^{\Delta 19/\Delta 19}$ (N=2) and *dmist*$^{i8/i8}$ (N=4) fish relative to wild type and heterozygous mutant siblings, as measured by fluorescence intensity of Sodium Green, normalized to the sample mean intensity. Crosses show mean ± SEM. *p<0.05, **p<0.01, one-way ANOVA

H) Under baseline conditions, brain sodium levels are significantly elevated in *dmist*$^{i8/i8}$ fish at night but not during the day, as measured by fluorescence intensity with Sodium Green. Crosses show mean ± SEM. *p<0.05, **p<0.01, one-way ANOVA

Figure S1. A viral insertion screen for sleep-wake regulators

A) Schematic of screening strategy. Candidate genes were selected from a list of 904 mammalian genes encoding protein classes most often linked to behavioural regulation, including 1) genes previously implicated in sleep and circadian rhythms; 2) G-protein coupled receptors; 3) neuropeptide ligands; 4) channels; and 5) proteins involved in post-translational regulation, such as de-ubiquitinating enzymes (Supplemental Data 1). tBLASTN of the human protein sequences identified 1162 zebrafish orthologs (Zv6), of which 702 (60.4%) had viral inserts mapped in the 'Zenemark' zebrafish viral insertion library (Varshney et al., 2013). Sperm harbouring viral insertions in 25 loci were successfully used for *in vitro* fertilization and propagated to the F3 generation for screening. F3 larvae from single family F2 in-crosses were monitored on a 14hr:10hr light:dark cycle from 4-7dpf using videography and genotyped at the end of the experiment.

B-C) Histogram of total daytime sleep (B) and average daytime waking activity (C) normalized as standard deviations from mean (Z-score) of all the viral-insertion lines tested (including heterozygous *vir*/+ and homozygous *vir/vir*). Line 10543 (renamed *dreammist*) exhibited decreased daytime sleep and increased daytime activity.

Figure S2. *dmist*$^{vir/vir}$ fish are hyperactive and have normal circadian rhythms.

A) Free-running circadian period length of locomotor activity of fish that were entrained until 5 dpf in a 14hr:10hr light:dark cycle and then shifted to constant darkness, and quantified for 48 hours after the shift to darkness, shows no difference between *dmist*$^{vir/vir}$ larvae and their sibling controls. p>0.05, one-way ANOVA

B-C) Representative 48hr sleep (B) and waking activity (C) traces of progeny from *dmist*$^{vir/+}$ in-cross following the transition from a 14hr:10hr light:dark cycle to constant dark conditions. Light and dark grey blocks show subjective day and night, respectively. Data are mean ± SEM.

D) Quantitative RT-PCR time-course before (light) and after (grey) transfer into constant dark demonstrates that *dmist* mRNA levels do not oscillate with a circadian period, unlike *per1* mRNA which does. n=3 replicates per timepoint. Expression is normalized to circadian time 3. Data are mean ± SEM.

Figure S3. *dmist* is enriched in neurons and requires the signal peptide cleavage site for membrane localisation.

A) Relative expression level of *dmist* transcript from RNA sequencing of 6dpf *dmist*$^{vir/vir}$ and *dmist*$^{+/+}$ siblings. Z-score calculated by subtracting mean expression and normalising by the standard deviation across all expressed transcripts (27,243 transcripts). Data show mean ± SEM from 3 independent biological replicates. **p<0.01 Student's t-test.

B) 3' and 5' RACE identify a long (1100bp) and short (215bp) 3'UTR variant in *dmist_Dr*, and a long 3'UTR (1050bp) in *Dmist_Mm*. The purple arrow indicates the ISH probe used in Figure 2D.

C) *dmist_Dr* sense probe at 24hpf shows no detectable expression.

D) Percentage identity matrix comparing *Dmist* homologues across 6 vertebrate species (100%=magenta; >70%=purple; >50%=cyan; <50%=green).

E) Hierarchical clustering of RNAseq dataset of 6 different cell types isolated from the developing (E13.5) mouse brain (Zhang et al., 2014) and post-hoc identification of *Dmist_Mm*. Data standardized by subtracting the mean expression and normalizing by the standard deviation across all expressed transcripts in each cell type (column). *Dmist_Mm* (green arrow) co-clusters with genes highly expressed in neurons (green shaded branches).

F) Pearson rank correlation of canonical cell-type markers with *Dmist_Mm* shows high co-expression with neuronal markers compared to astroglial markers. Data are mean ± SEM *p<0.05, **p<0.01; Kruskal-Wallis, Dunn-Sidak post-hoc test.

G-I) Predicted processing of Dmist to its mature form in the plasma membrane (G) and C-terminal GFP fusion to Dmist is predicted to localise to the membrane (H) The black triangle represents the cap. However, a mutation (A22W) at the signal peptide cleavage site (I) is

predicted to inhibit signal peptide cleavage and so prevent proper subcellular localisation of the mature protein.

Figure S4. CRISPR-generated *dmist* mutants have altered sleep and arousal phenotypes

A) Quantitative RT-PCR shows *dmist*$^{i8/i8}$ larvae have reduced *dmist* mRNA levels, suggesting that *dmist*^{i8} transcripts undergo nonsense mediated decay. Data are mean ± SD of three biological replicates. **p<0.01; one-way ANOVA, Tukey's post-hoc test.

B) Relative expression level of *dmist* transcript from RNA sequencing of 6dpf *dmist*$^{i8/i8}$ and *dmist*$^{+/+}$ siblings. Z-score calculated by subtracting mean expression and normalising by the standard deviation across all expressed transcripts. Data are mean ± SEM for 3 independent biological replicates. **p<0.01, Student's t-test.

C) Effect size of change in sleep after 1 hour 5mM PTZ treatment (and washout) compared to vehicle treated controls (error bars show 95% confidence intervals). *p<0.05, one-way ANOVA.

D) Cumulative probability distribution of the all night-time swimming speeds in representative adult tracking experiment. The dashed lines show the half max (0.5 probability) for each curve. n indicates number of fish. *p<0.05; Kolmogorov-Smirnov test.

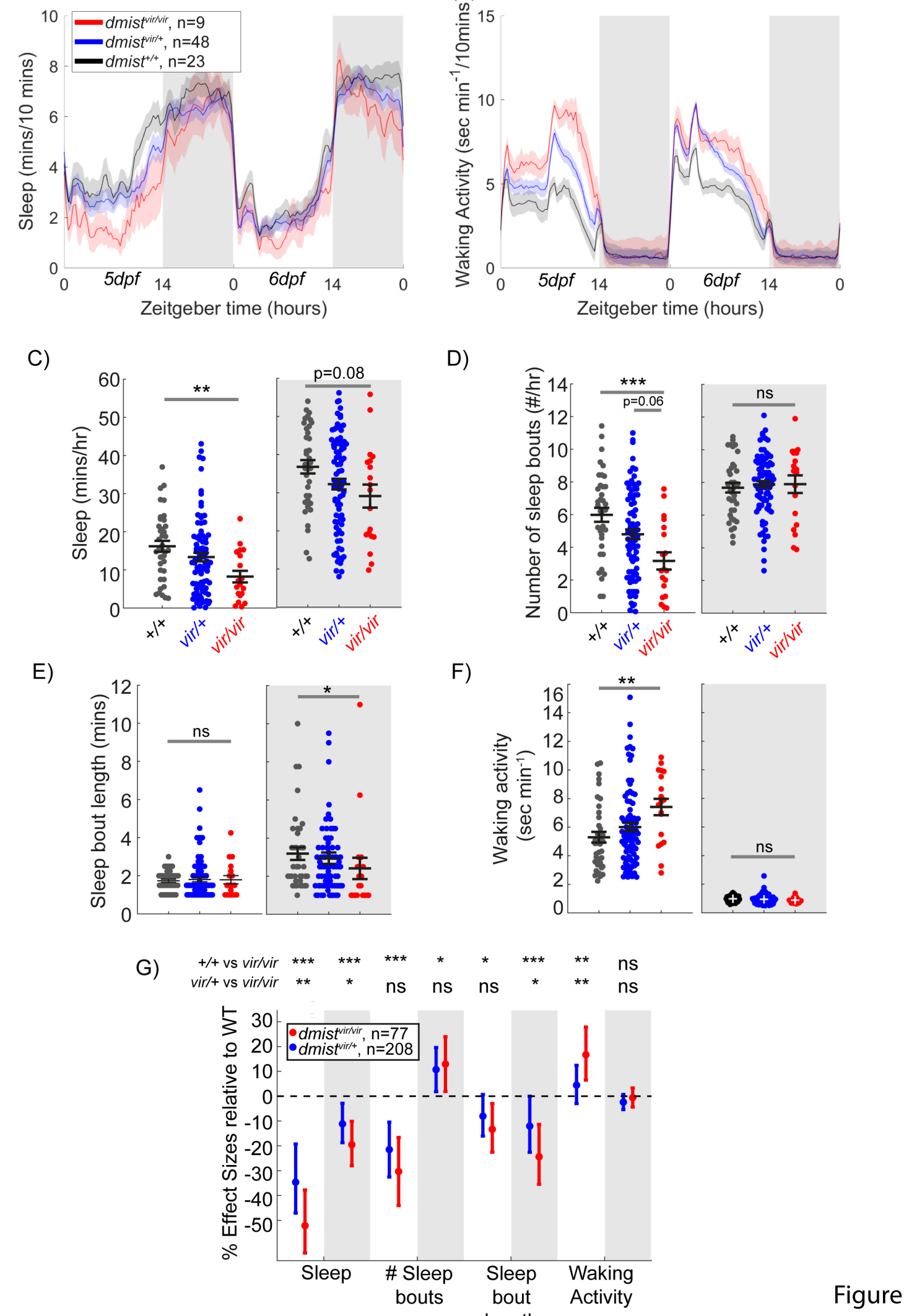

Figure 1

A)

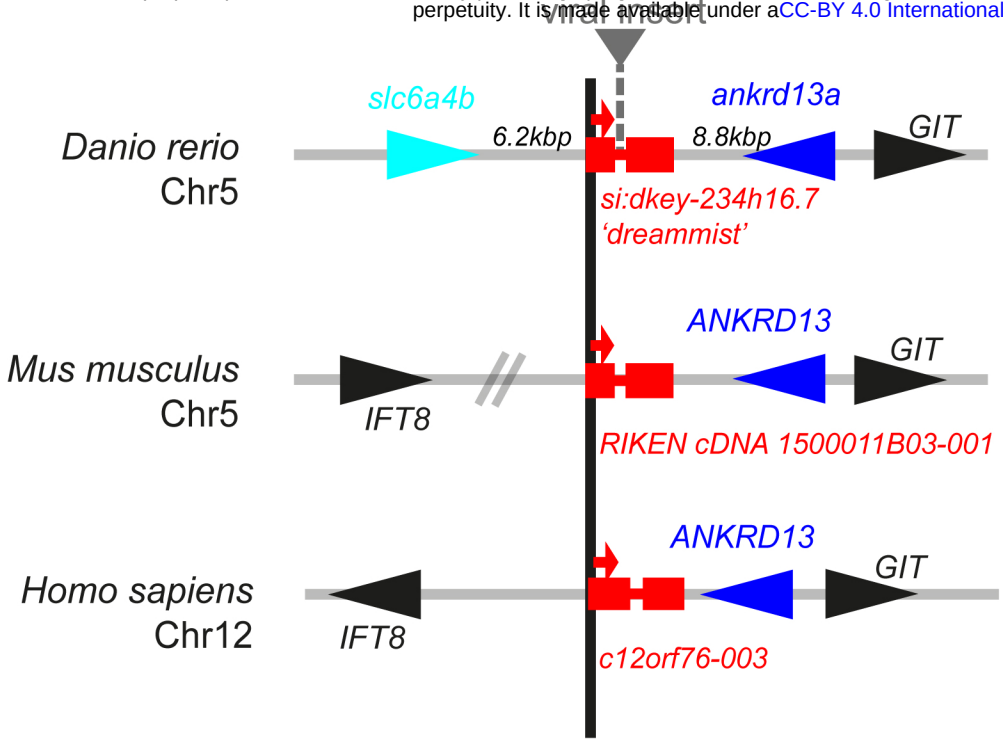

B)

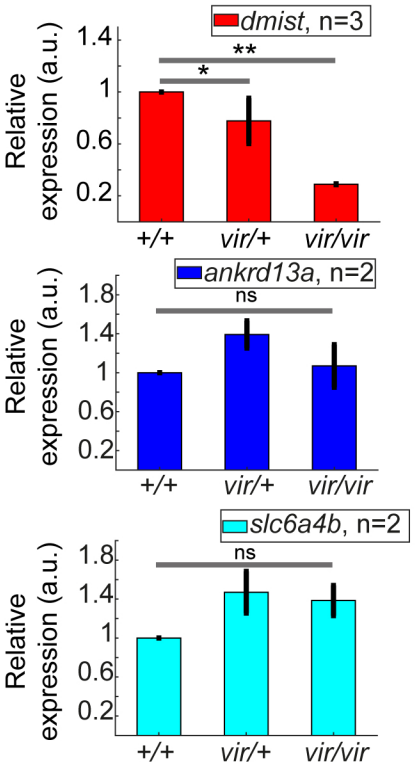

C)

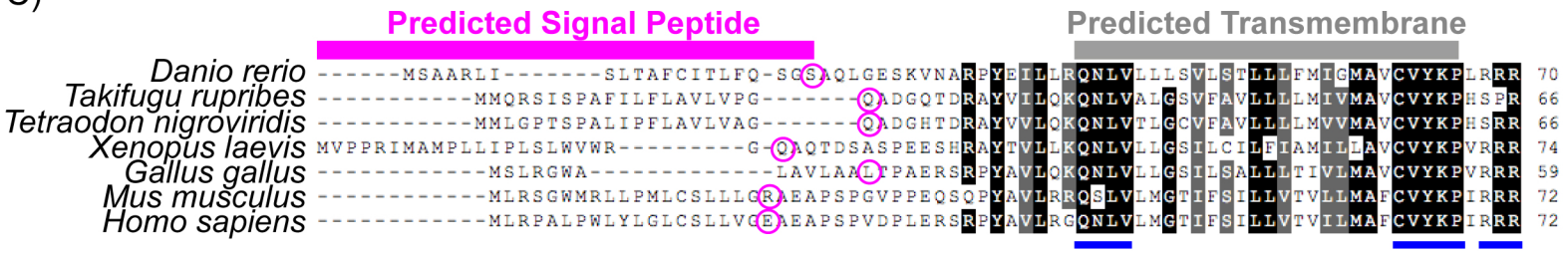

D)

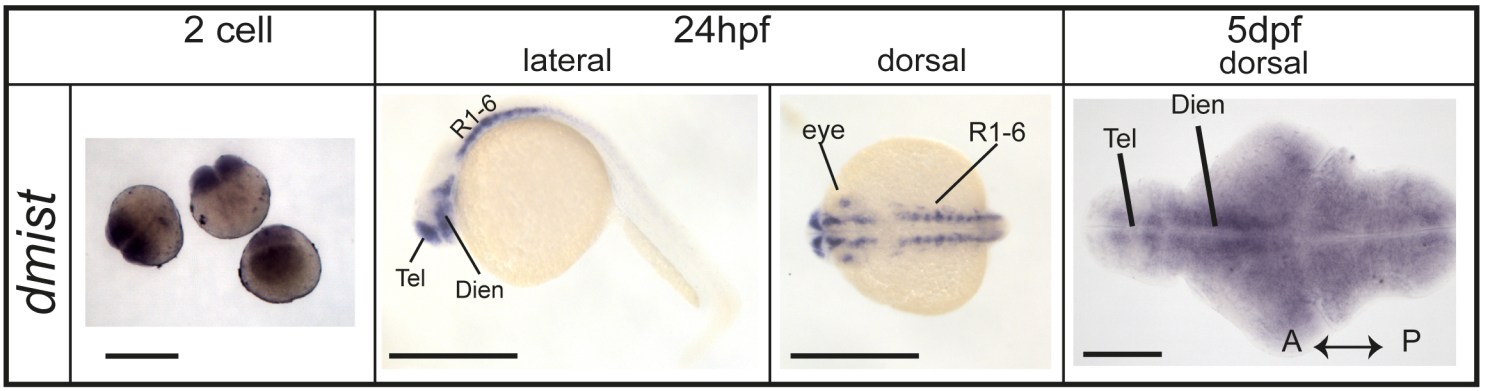

E)

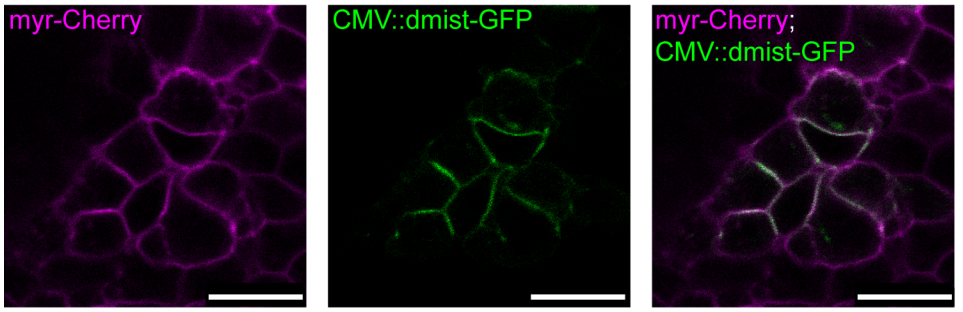

F)

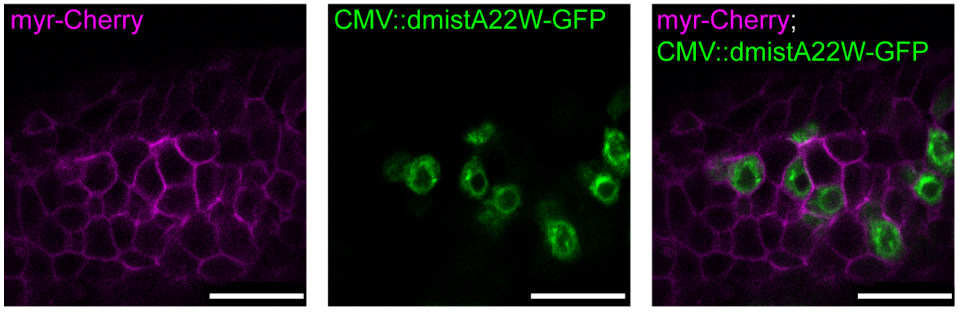

Figure 2

A)

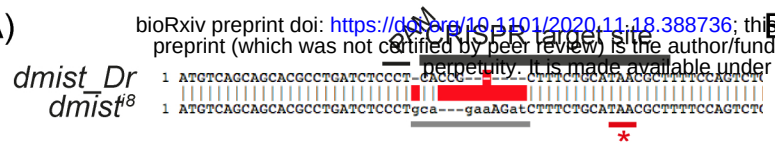

B)

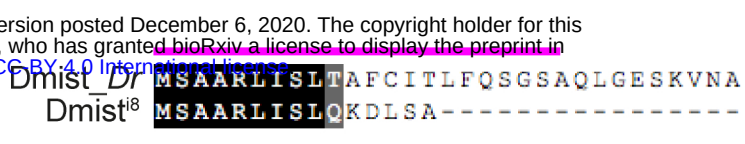

C)

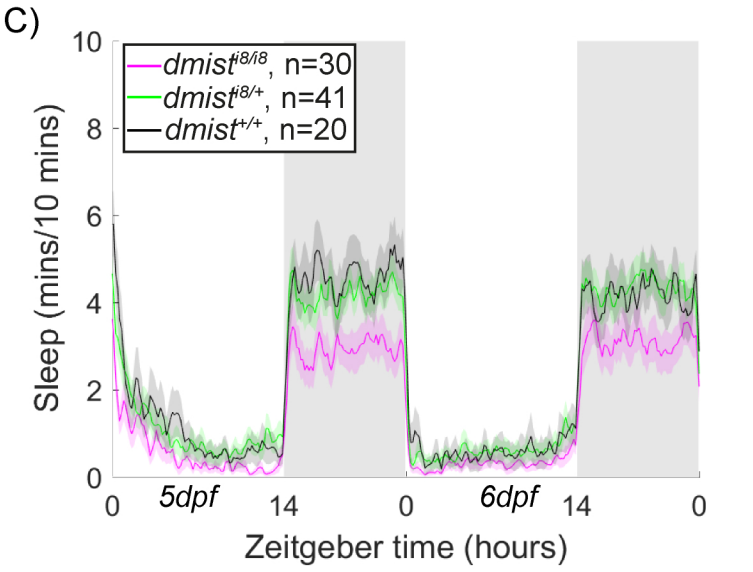

D)

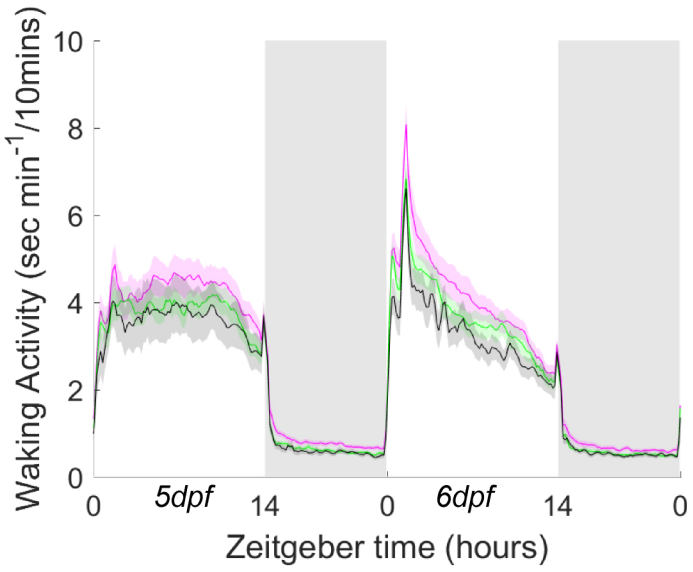

E)

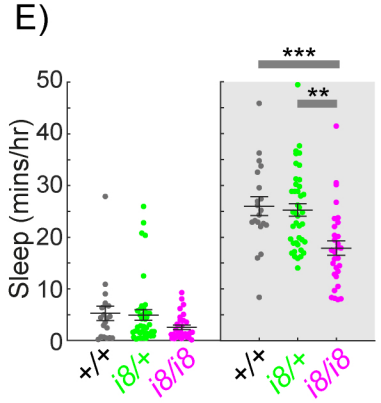

F)

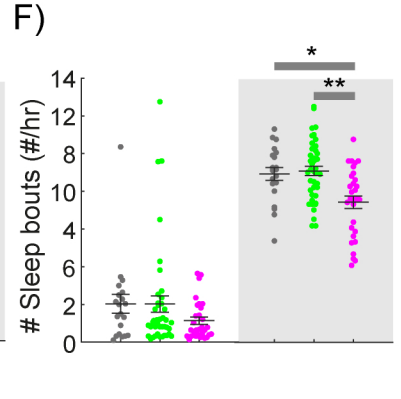

G)

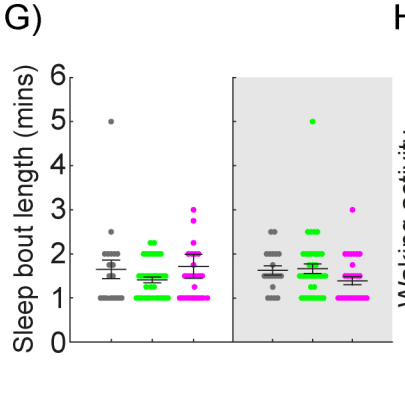

H)

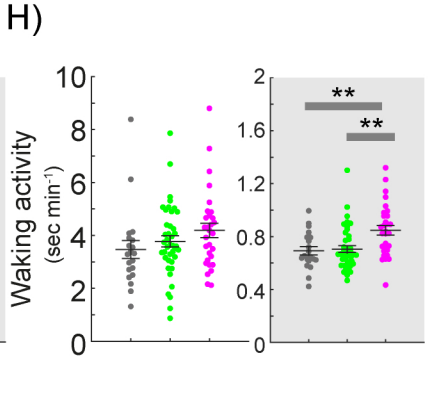

I)

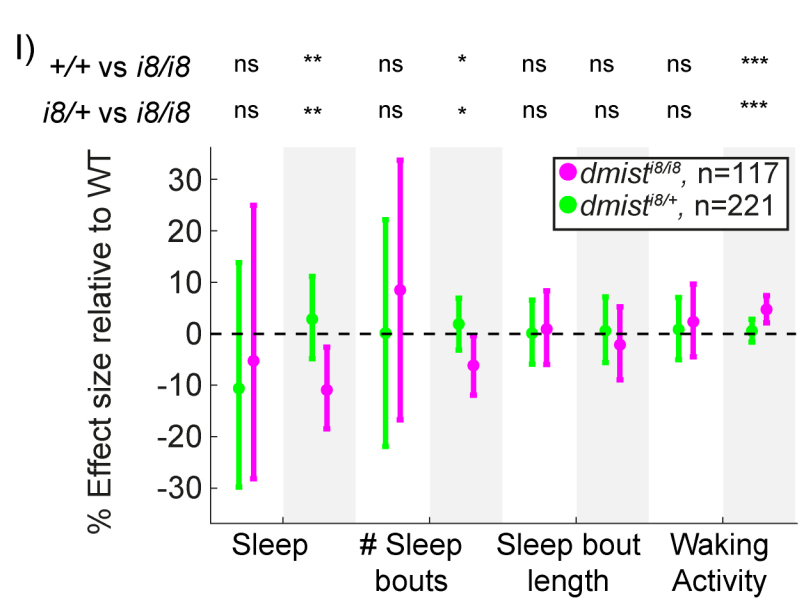

J)

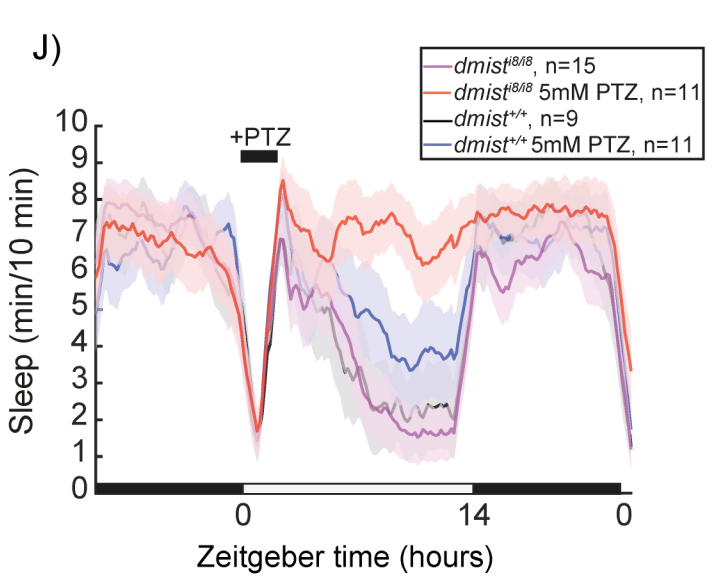

K)

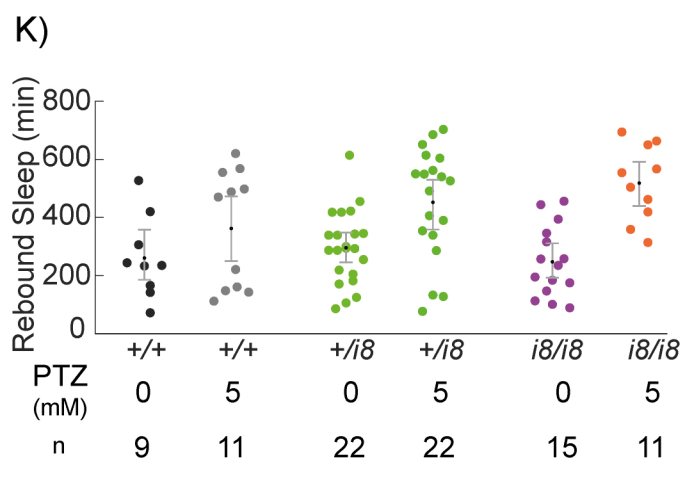

L)

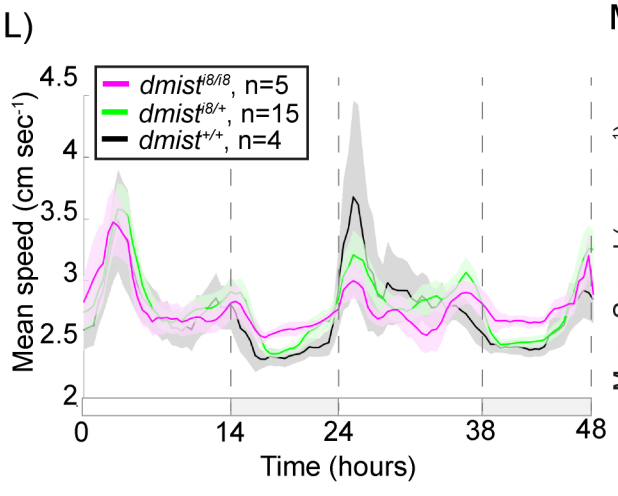

M)

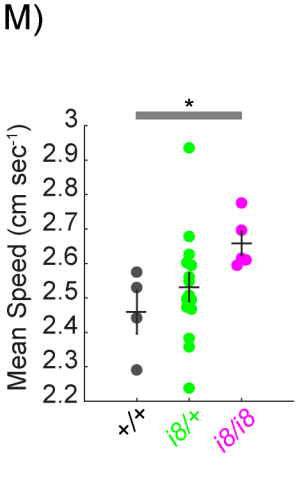

FIgure 3

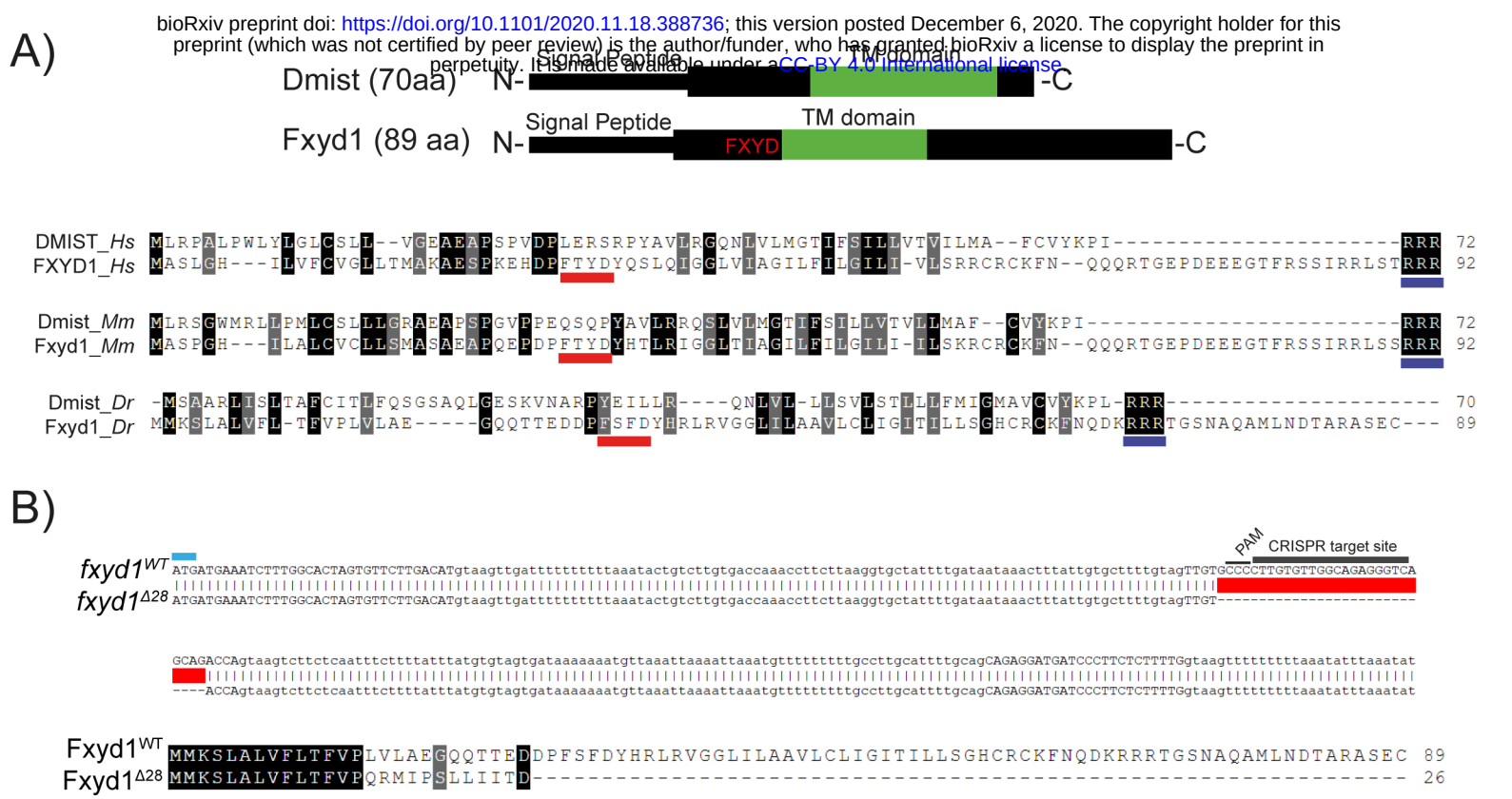

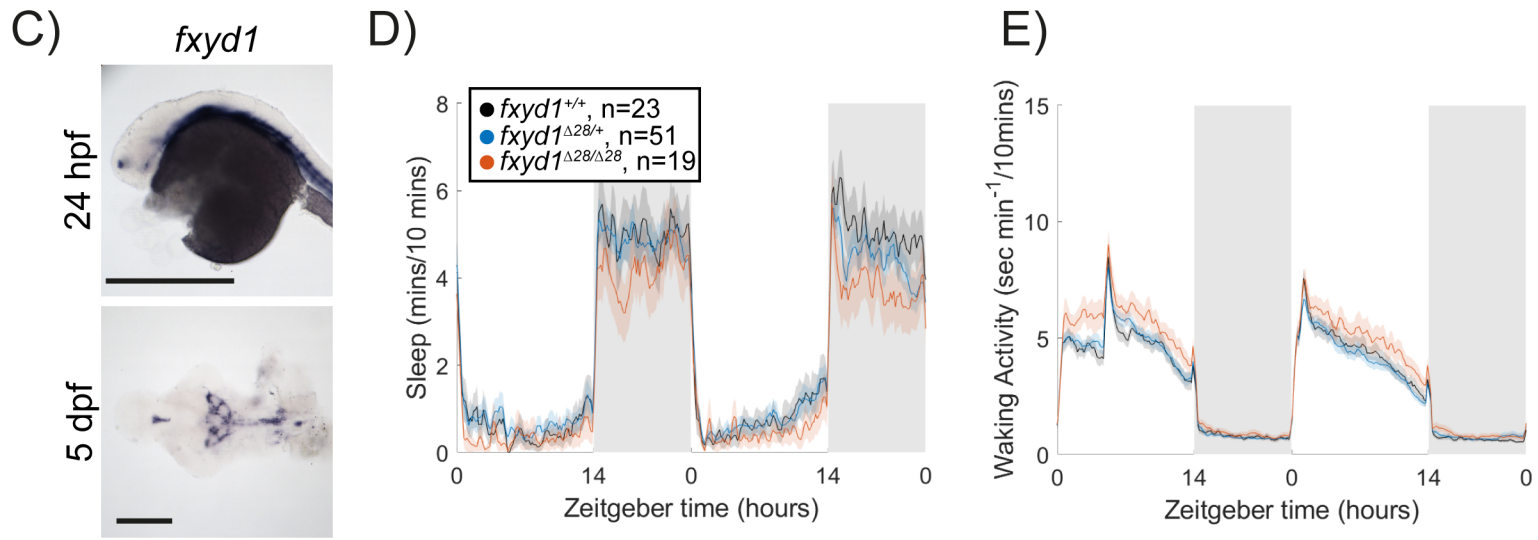

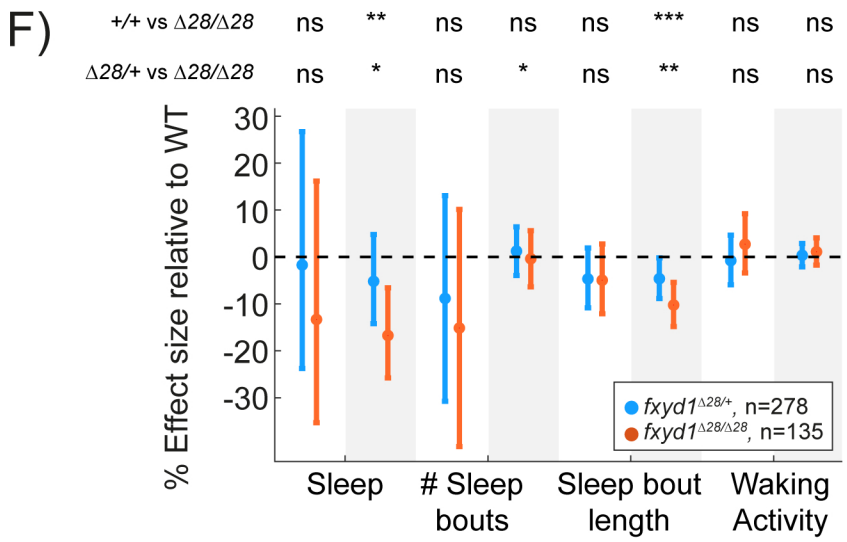

FIgure 4

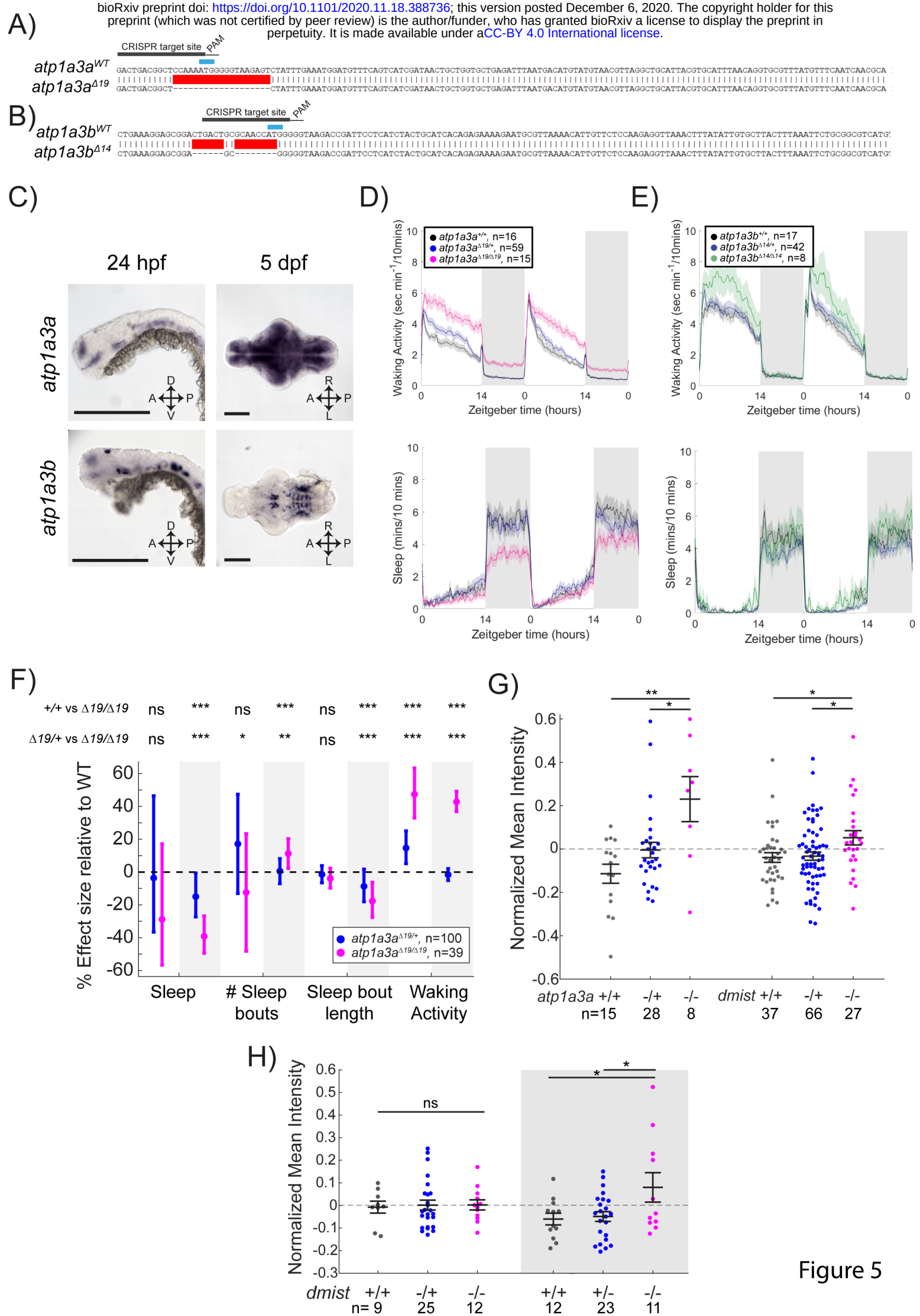

Figure 5

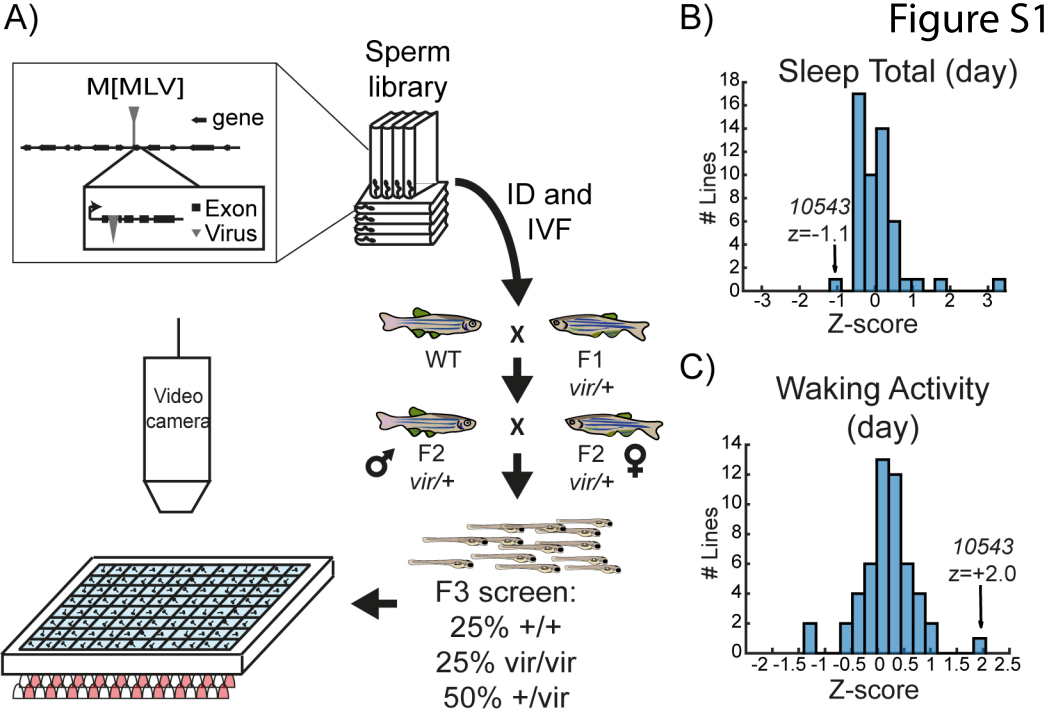
A)
M[MLV]
gene
Exon
Virus
Sperm library
ID and IVF
WT
F1
vir/+
F2
vir/+
F2
vir/+
Video camera
F3 screen:
25% +/+
25% vir/vir
50% +/vir
B)
Figure S1
Sleep Total (day)
Lines
10543
z=-1.1
Z-score
C)
Waking Activity (day)
Lines
10543
z=+2.0
Z-score

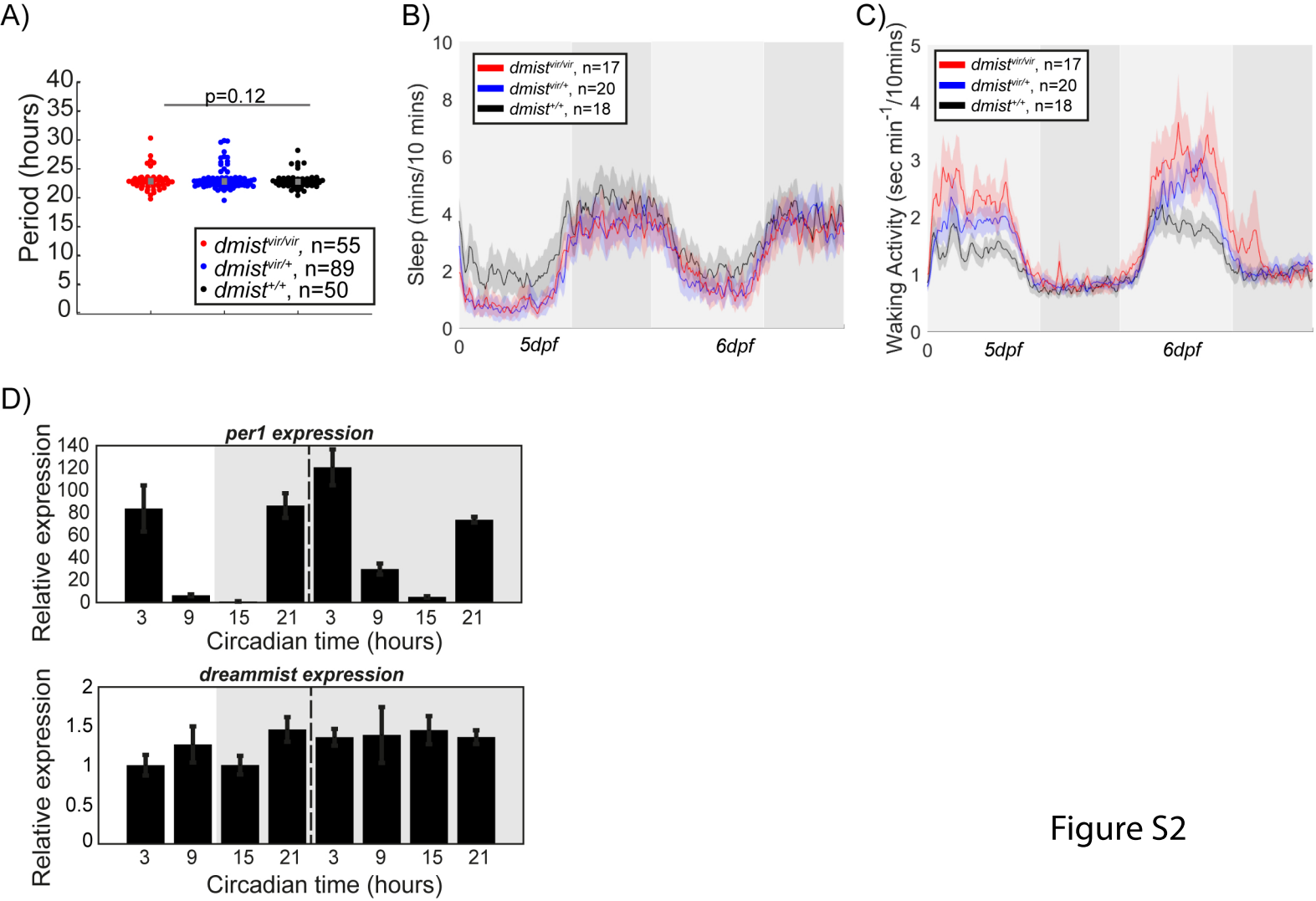
A)
Period (hours)
p=0.12
dmist vir/vir, n=55
dmist vir/+, n=89
dmist +/+, n=50
B)
Sleep (mins/10 mins)
dmist vir/vir, n=17
dmist vir/+, n=20
dmist +/+, n=18
5dpf
6dpf
C)
Waking Activity (sec min-1/10mins)
dmist vir/vir, n=17
dmist vir/+, n=20
dmist +/+, n=18
5dpf
6dpf
D)
per1 expression
Relative expression
Circadian time (hours)
dreammist expression
Relative expression
Circadian time (hours)

Figure S2

Figure S3

A)

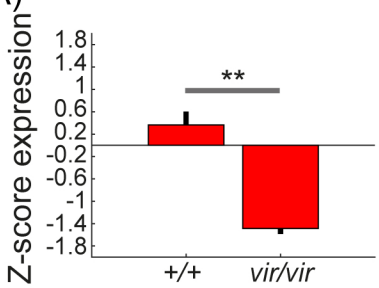

B)

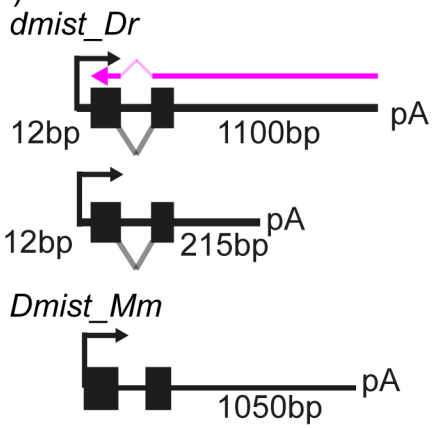

C)

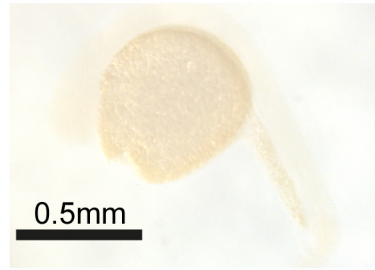

D)

Species	*Danio rerio*	*Takifugu rupibes*	*Xenopus laevis*	*Gallus gallus*	*Mus musculus*	*Homo sapiens*
Danio rerio	100.00	56.82	52.08	61.36	43.75	47.92
Takifugu rupibes	56.82	100.00	52.27	54.55	38.64	45.45
Xenopus laevis	52.08	52.27	100.00	68.18	46.00	52.00
Gallus gallus	61.36	54.55	68.18	100.00	65.91	72.73
Mus musculus	43.75	38.64	46.00	65.91	100.00	84.31
Homo sapiens	47.92	45.45	52.00	72.73	84.31	100.00

E)

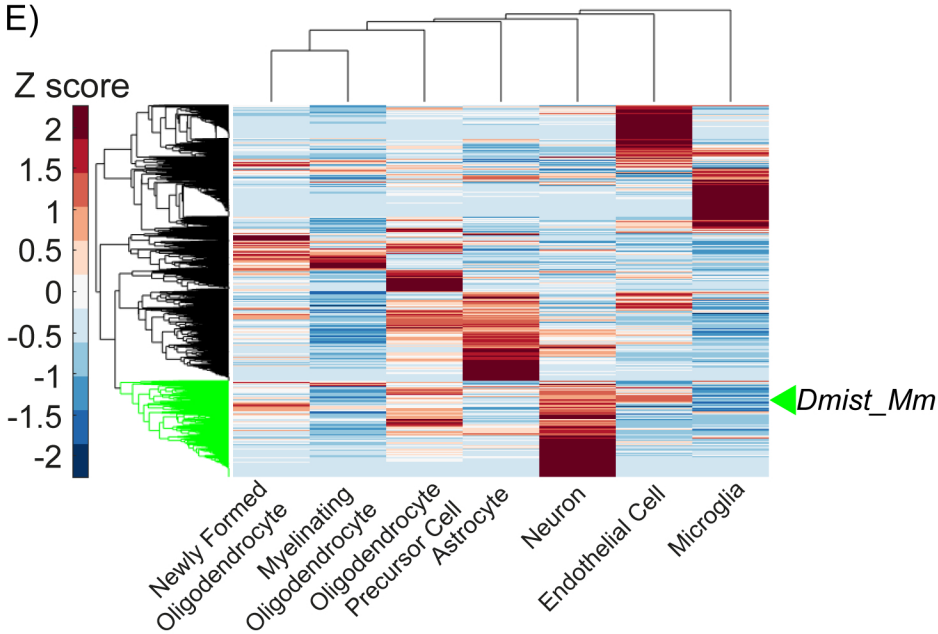

F)

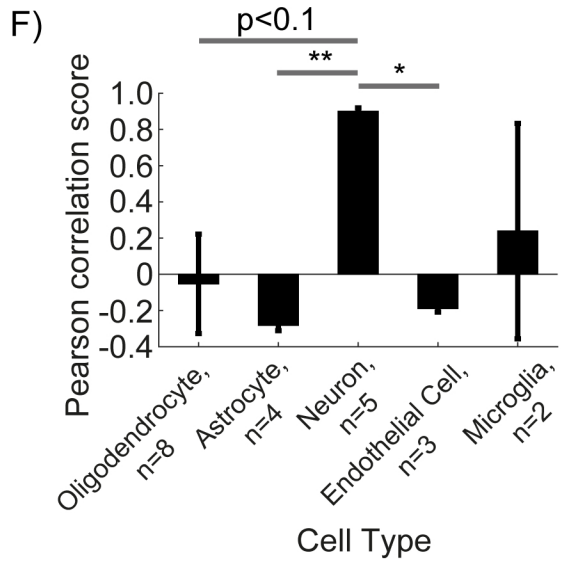

G)

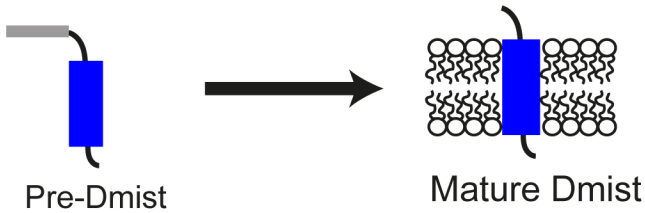

H)

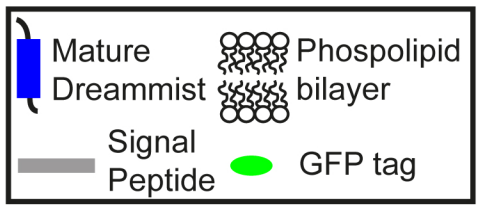

I)

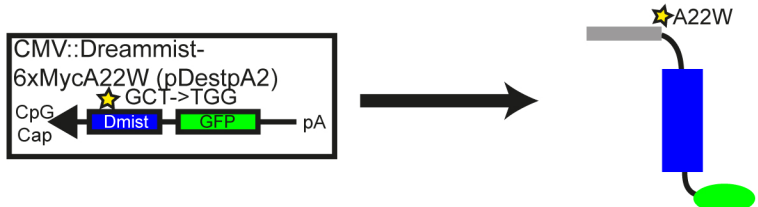

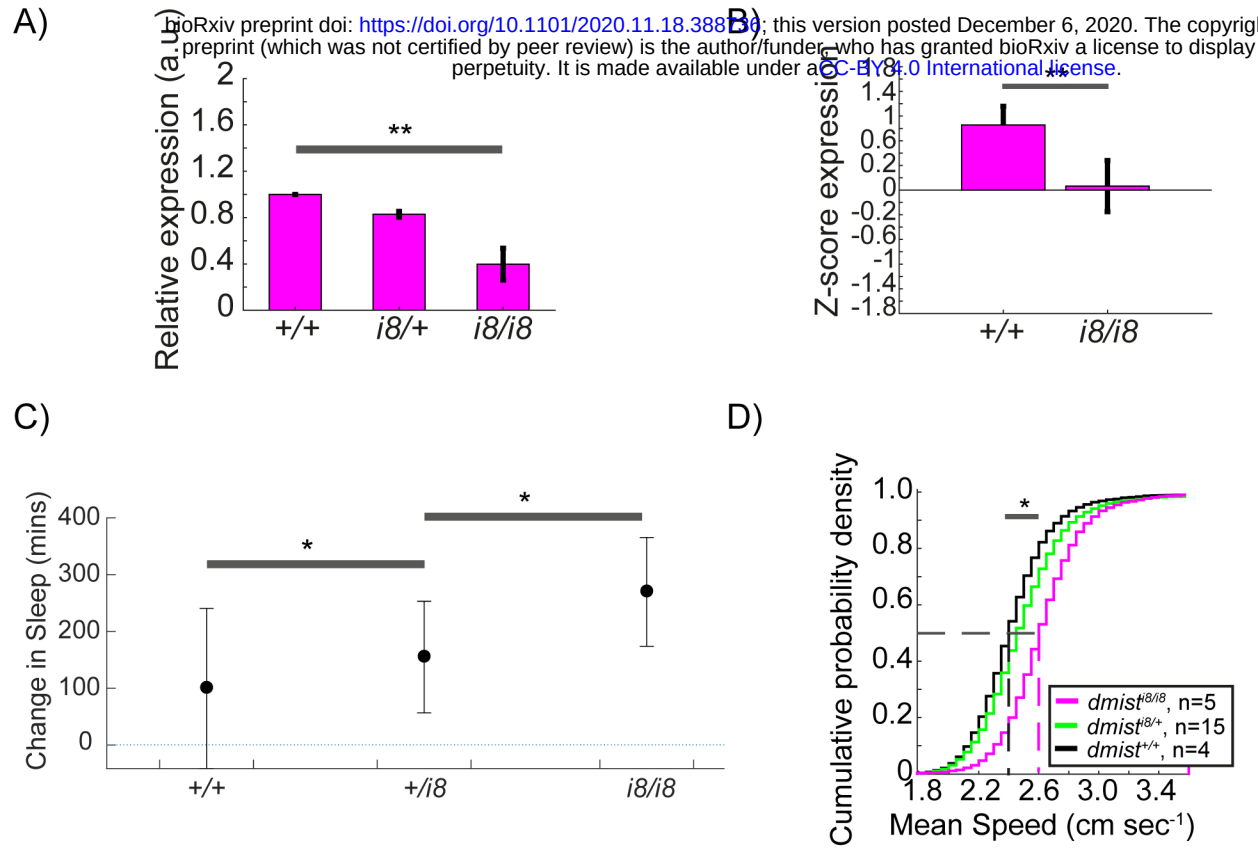

Figure S4